

Thermal kaons production in the relativistic heavy ions collision

I. Zakout, W. Greiner

*Institut für Theoretische Physik, J. W. Goethe Universitaät,
Robert-Mayer-Straße 8-10, Postfach 11 19 32,
D-60054 Frankfurt am main, Germany*

H. R. Jaqaman

*Physics Department, Bethlehem University,
P.O. Box 9 Bethlehem, Palestinian Authority*

Abstract

We study the thermal production of kaons in hot and dense symmetric and asymmetric hypernuclear matter in the context of the modified quark-meson coupling model. All the baryon species and kaons are treated as MIT bags that interact with each other via the scalar mesons σ, σ^* and the vector mesons ω, ϕ as well as the isovector meson ρ . Furthermore, in our calculations, we use realistic sets of hyperon-hyperon (or YY) interactions based on several versions of Nijmegen core potential models. We consider a system of strange hadronic matter and kaons but with zero total net strangeness of the system and conserved small negative fraction of the isospin-charge. We find strange baryons as well as kaons are produced abundantly when the temperature increases and approaches the critical temperature for the phase transition to the quark-gluon plasma. Our results show that the kaons are produced only thermally in the symmetric and asymmetric hypernuclear matter and there is no signature for the onset of kaon condensation in the relativistic heavy ions collision. The kaons appear in the system only by thermal production. However, when the system cools down strange hadrons could survive.

I. INTRODUCTION

The quark-meson coupling (QMC) model incorporates the quark-gluon degrees of freedom while respecting the established model based on the hadronic degrees of freedom in nuclei. It describes nuclear matter as a collection of non-overlapping MIT bags interacting through self-consistent exchange of scalar σ, σ^* and vector mesons ω, ϕ as well as the isovector meson ρ in the mean field approximation with the mesonic fields directly coupled to the quarks[1]. In the so-called modified quark-meson coupling model (MQMC)[2, 3, 4], it has been suggested that including a medium-dependent bag parameter is essential for the success of relativistic nuclear phenomenology. The density-dependence of the bag parameter is introduced by coupling it to the scalar mesonic field[2, 4]. We have used the MQMC model to study the properties of nuclear matter and quark deconfinement at finite temperature[5, 6, 7] and the phase transition from the hadronic phase to the quark-gluon plasma [7, 8]. We have studied the properties of neutron stars in the context of MQMC[9].

The scalar meson σ with mass 550 MeV is supposed to simulate the exchange of correlated pairs of pions and may represent a very broad resonance observed in $\pi\pi$ scattering, while the vector meson ω is identified with the actual meson having a mass of about 780 MeV. The σ scalar and ω vector mesonic fields couple the up and down flavor. Also the additional scalar $\sigma^*(s\bar{s})$ and vector $\phi(s\bar{s})$ mesonic fields are actual mesons with masses 975 and 1020 MeV, respectively. They are introduced to couple the strange flavor quark. Similarly, the mesonic isovector field ρ which is essential for isospin charged nuclear matter is an actual meson with mass 770. It exchanges the non-strange flavor quark.

We assume pure strange hadronic matter to consist of the members of the SU(3) baryon octet and the kaons doublet. The baryon octet is comprised of $(p, n, \Lambda, \Sigma^+, \Sigma^0, \Sigma^-, \Xi^0, \Xi^-)$ baryons while the kaon doublet is comprised of (K^+, K^0) mesons. In heavy ion collisions the total net strangeness of the system is conserved during the collision. If the quark-gluon plasma is produced during the collision the net strangeness for the hadronic phase may not be conserved but the total net strangeness for both the hadronic and quark-gluon phases shall be conserved.

Various calculations and models predict that metastable strange systems with strangeness fractions of order one and charge neutrality might exist in the hadronic phase at densities between two and three times nuclear matter saturation density[10, 11]. However, the pre-

dicted phenomenon of metastability of strange hadronic matter and the actual values of the binding energy depend specifically on the partly unknown hyperon potentials assumed in dense matter[10, 11, 12, 13]. Recently, unconstrained Relativistic Mean Field calculations of the charge-neutral strangeness-rich hadronic system have been carried with two sets of hyperon-hyperon (or YY) potentials, the first set is determined from the Nijmegen hard-core potential Model D[14], and the second set corresponds to the potentials obtained in a recent SU(3) extension of the Nijmegen soft-core potential Model NSC97[15, 16, 17, 18]. The differences between these two sets are essentially attributable to the extremely attractive $\Sigma\Sigma$ and $\Xi\Xi$ interactions in the second set which allow for the possibility of deeply bound nuclear matter with hyperons[19].

In the present work, we shall study the production of kaons in neutral as well as weakly isospin charged strange hadronic matter at finite temperature. We shall adopt realistic phenomenological fitting parameters which are calculated from the potential models. The outline of the paper is as follow. In sec. II we write the equation of state. Then in section III, we present two different set of the fitting parameters for YY potentials. In section IV, we give our results and conclusions. Finally, we summarize our conclusions in section V.

II. EQUATION OF STATE

The quark field $\psi_q(\vec{r}, t)$ inside a bag of radius R_i representing a baryon of species i satisfies the Dirac equation

$$\left[i\gamma^\mu \partial_\mu - m_q^0 + (g_{q\sigma}\sigma - g_{q\omega}\omega_\mu\gamma^\mu) + (g_{q\sigma^*}\sigma^* - g_{q\phi}\phi_\mu\gamma^\mu) - g_{q\rho}\frac{1}{2}\vec{\tau}\cdot\vec{\rho}_\mu\gamma^\mu \right] \psi_q(\vec{r}, t) = 0, \quad (1)$$

where m_q^0 is the current mass of a quark of flavor q . The current quark masses are taken, for the up and down flavor quarks, to be $m_u = m_d = 0$ while for the strange flavor $m_s = 150\text{MeV}$. Inclusion of small current quark masses for the non-strange flavors or other values for the strange flavor leads only to small numerical refinements of the present results. In the mean field approximation the meson fields are treated classically and the space like components of the vector fields vanish for infinite systems due to rotational invariance. As a result we get $\omega_\mu\gamma^\mu = \langle \omega_0 \rangle \gamma^0 = \omega\gamma^0$ and $\phi_\mu\gamma^\mu = \langle \phi_0 \rangle \gamma^0 = \phi\gamma^0$ and $\vec{\tau}\cdot\vec{\rho}_\mu\gamma^\mu = \tau_3 \langle \rho_0^3 \rangle \gamma^0 = \tau_3\rho\gamma^0$.

The non strange (up and down) flavor quarks are coupled to the scalar $\sigma(550)$ and vector $\omega(780)$ and isovector $\rho(980)$ mesons while the strange flavor quarks are coupled to $\sigma^*(975)$

and $\phi(1020)$.

For a given value of the bag radius R_i and the scalar fields σ and σ^* , the quark momentum x_{qi} is determined by the boundary condition of confinement which, for quarks of flavor q in a spherical bag, reduces to $j_0(x_{qi}) = \beta_{qi}j_1(x_{qi})$, where

$$\beta_{qi} = \sqrt{\frac{\Omega_{qi}(\sigma, \sigma^*) - R_i m_q^*}{\Omega_{qi}(\sigma, \sigma^*) + R_i m_q^*}}. \quad (2)$$

We have defined the effective quark mass inside the bag as

$$m_q^* = m_q^0 - g_{q\sigma}\sigma - g_{q\sigma^*}\sigma^*, \quad (3)$$

and the effective quark energy is given by

$$\Omega_{qi}(\sigma, \sigma^*)/R_i = \sqrt{(x_{qi}/R_i)^2 + m_q^{*2}}. \quad (4)$$

The bag energy is given by

$$E_{\text{bag}_i} = E_{\text{quarks}_i} - \frac{Z_i}{R_i} + \frac{4\pi}{3}R_i^3 B_i(\sigma, \sigma^*), \quad (5)$$

where

$$E_{\text{quarks}_i} = \sum_q^{n_q} \frac{\Omega_{qi}(\sigma, \sigma^*)}{R_i} \quad (6)$$

is the total constituent quarks kinetic energy inside the bag and $\frac{Z_i}{R_i}$ term is the zero-point energy of the quarks and $B_i(\sigma, \sigma^*)$ is the medium-dependent bag parameter.

We would like to emphasize here that we didn't take into account the thermal excitation of the constituent quarks inside the bag[5, 6, 7, 20]. In Refs.[5, 6, 7, 20], the total constituent quarks kinetic energy with thermal excitations of the populated quarks is given by

$$E_{\text{quarks}_i} = \sum_q^{n_q} \frac{\Omega_{qi}(\sigma, \sigma^*)}{R_i} \left(f_q[\epsilon_q^* - \mu_q] - f_q[\bar{\epsilon}_q^* + \mu_q] \right) \quad (7)$$

where $f_q[\epsilon_q^* - \mu_q]$ and $f_q[\bar{\epsilon}_q^* + \mu_q]$ are the Fermi-Dirac quark and antiquark distribution functions, respectively. The constituent quark effective energy is given by

$$\epsilon_q^* = \frac{\Omega_{qi}(\sigma, \sigma^*)}{R_i} + (g_{q\omega}\omega + g_{q\phi}\phi + \frac{1}{2}g_{q\rho}\tau_3\rho) \quad (8)$$

and

$$\bar{\epsilon}_q^* = \frac{\Omega_{qi}(\sigma, \sigma^*)}{R_i} - (g_{q\omega}\omega + g_{q\phi}\phi + \frac{1}{2}g_{q\rho}\tau_3\rho) \quad (9)$$

In this construction, the constituent quark chemical potential μ_q is determined from the constraint

$$n_q = \sum_q^{n_q} f_q [\epsilon_q^* - \mu_q] - \bar{f}_q [\bar{\epsilon}_q^* + \mu_q] \quad (10)$$

where n_q is the number of the constituent quarks (antiquarks) inside the bag. This constraint, fortunately, gives $f_q \approx 1$ and $\bar{f}_q \approx 0$ in the actual numerical calculations. We have found that adopting Eq.(6) rather Eq.(7) in the calculations doesn't affect the results given in Refs[5, 6, 7]. Therefore, the thermal excitations of the populated quarks inside the bags in that construction is negligible[5, 6, 7].

In the simple QMC model, the bag parameter (constant) is taken as B_0 corresponding to its value for a free baryon. The medium effects are taken into account in the MQMC model[2, 3] by coupling the bag parameter to the scalar meson fields. In the present work we use the following generalized ansatz for the coupling of the bag parameter to the scalar fields σ and σ^* [7, 8, 9]:

$$B_i(\sigma, \sigma^*) = B_0 \exp \left[-4 \left(g_{i\sigma}^{\text{bag}} \sigma + g_{i\sigma^*}^{\text{bag}} \sigma^* \right) / M_i \right] \quad (11)$$

with $g_{i\sigma}^{\text{bag}}$ and $g_{i\sigma^*}^{\text{bag}}$ as additional coupling constants to be fitted from the phenomenology. In Ref.[13], the bag parameter has been considered to couple to the non strange σ scalar field but not to the strange σ^* scalar field. The spurious center-of-mass energy is subtracted to obtain the effective baryon mass

$$M_i^* = \sqrt{E_{\text{bag}_i}^2 - \langle p_{\text{cm}}^2 \rangle_i}, \quad (12)$$

where

$$\langle p_{\text{cm}}^2 \rangle_i = \sum_q^{n_q} x_{qi}^2 / R_i^2. \quad (13)$$

The bag radii R_i and R_k for baryon i and kaon k species, respectively, are obtained through the minimization of the baryon mass with respect to the bag radius[1]

$$\frac{\partial M_i^*}{\partial R_i} = 0. \quad (14)$$

The coupling of the scalar mean fields σ and σ^* with quarks in the non overlapping MIT bag through the solution of the point-like Dirac equation should be taken into account to

satisfy the self-consistency condition. However, this constraint is essential to obtain the correct solution of the scalar mean field σ and σ^* . We think the discrepancy between our results in Ref.[5] and those in Ref.[20] is due to the coupling of the quark with the scalar mean fields σ, σ^* in the framework of the point like Dirac equation. The differentiation of the effective hadrons species with respect to σ gives

$$\frac{\partial M_i^*}{\partial \sigma} = \frac{E_{\text{bag}_i} \left(\frac{\partial E_{\text{bag}_i}}{\partial \sigma} \right)_{\sigma^*} - \frac{1}{2} \left(\frac{\partial \langle p_{\text{cm}}^2 \rangle_i}{\partial \sigma} \right)_{\sigma_*}}{M_i^*} \quad (15)$$

where

$$\left(\frac{\partial E_{\text{bag}_i}}{\partial \sigma} \right)_{\sigma^*} = \sum_q \left(\frac{\partial E_{\text{bag}_i}}{\partial \Omega_{qi}} \right) \left(\frac{\partial \Omega_{qi}}{\partial \sigma} \right) + \left(\frac{\partial E_{\text{bag}_i}}{\partial \sigma} \right)_{\Omega_{qi}} \quad (16)$$

$$\frac{\partial E_{\text{bag}_i}}{\partial \Omega_{qi}} = \sum_{q'} \frac{\delta_{q'q}}{R_i} \quad (17)$$

and

$$\left(\frac{\partial E_{\text{bag}_i}}{\partial \sigma} \right)_{\Omega_{qi}} = \frac{4\pi}{3} R_i^3 \frac{\partial B_i(\sigma, \sigma^*)}{\partial \sigma} \quad (18)$$

The $\frac{\partial \Omega_{qi}}{\partial \sigma}$ depends on x_{qi} . Its solution is obtained from the point-like Dirac equation for the quarks and must satisfy the required boundary condition as well as the confinement on the bag surface[1, 2]. It reads

$$\frac{1}{R_i} \frac{\partial \Omega_{qi}}{\partial \sigma} = -g_{q\sigma} \langle \bar{\psi}_i | \psi_i \rangle, \quad (19)$$

where

$$\langle \bar{\psi}_i | \psi_i \rangle = \frac{\Omega_{qi}/2 + m_q^* R_i (\Omega_{qi} - 1)}{\Omega_{qi} (\Omega_{qi} - 1) + m_q^* R_i / 2}. \quad (20)$$

Furthermore, the term for the spurious center-of-mass momentum correction reads

$$\frac{\partial \langle p_{\text{cm}}^2 \rangle_i}{\partial \sigma} = \frac{1}{R_i^2} \sum_q \frac{\partial x_{qi}^2}{\partial \sigma}, \quad (21)$$

where

$$\frac{\partial x_{qi}^2}{\partial \sigma} = \left(2\Omega_{qi} \frac{\partial \Omega_{qi}}{\partial \sigma} \right) + 2R_i^2 m_q^* g_{qi}. \quad (22)$$

Similar expressions can be obtained for the differentiation of the effective hadron (baryon and kaon) species mass with respect to the scalar mean field σ^* . The zero-point energy parameters Z_i of Eq.(4) are used to fit the actual masses of the free baryons $M_i = 939, 1116, 1193$ and 1315MeV and are found to be $Z_i=2.03, 1.814, 1.629$ and 1.505 for the N, Λ, Σ and Ξ hyperons respectively, corresponding to a free baryon bag parameter $B_0 = (188.1)^4\text{MeV}^4$ and a free nucleon bag radius $R_0 = 0.6\text{fm}$. The zero-point energy parameter Z_k is used to fit the actual mass of free kaon $M_k = 495 \text{ MeV}$ and is found $Z_k=1.170$.

The effective Fermi-energy for baryon and antibaryon species i reads

$$\epsilon_i^*(p) = \sqrt{p^2 + M_i^{*2}} + X_i \quad (23)$$

and

$$\bar{\epsilon}_i^*(p) = \sqrt{p^2 + M_i^{*2}} - X_i, \quad (24)$$

respectively, where

$$X_i = [g_{i\omega}\omega + g_{i\phi}\phi + g_{i\rho}I_{3i}\rho]. \quad (25)$$

The effective Bose-energy for kaon and antikaon species reads

$$\epsilon_k^*(p) = \sqrt{p^2 + M_k^{*2}} + X_k, \quad (26)$$

and

$$\bar{\epsilon}_k^*(p) = \sqrt{p^2 + M_k^{*2}} - X_k, \quad (27)$$

respectively, where

$$X_k = [g_{k\omega}\omega + g_{k\phi}\phi + g_{k\rho}I_{3k}\rho]. \quad (28)$$

The indices for kaon and antikaon species are given by $k = (K^+, K^0)$ and $\bar{k} = (K^-, \bar{K}^0)$, respectively.

The chemical potentials μ_i and μ_k for baryon species i and kaon species k read

$$\mu_i = B_i\mu_B + S_i\mu_S + Q_i\mu_Q, \quad (29)$$

and

$$\mu_k = S_k\mu_S + Q_k\mu_Q, \quad (30)$$

respectively. The quantum numbers B_i , S_i and Q_i are the baryon, strangeness and isospin quantum numbers, respectively. The baryon, strangeness, isospin-charge chemical potentials μ_B , μ_S and μ_Q , respectively, are determined from the constraints of total baryon, strange and isospin charge densities n_B Eq.(37), n_S^{Total} Eq.(38) and n_Q^{Total} Eq.(39), respectively.

The density for each baryon and antibaryon species reads

$$n_i = \frac{d_i}{(2\pi)^3} \int d^3p f[\epsilon_i^*(p) - \mu_i], \quad (31)$$

and

$$\bar{n}_i = \frac{d_i}{(2\pi)^3} \int d^3p f[\bar{\epsilon}_i^*(p) + \mu_i], \quad (32)$$

respectively, where $d_i = 2$ is the spin degeneracy for the octet baryon species. The Fermi-Dirac distribution function reads

$$f[x] = \frac{1}{(e^{x/T} + 1)}. \quad (33)$$

The density for each kaon and antikaon species reads

$$n_k = \frac{d_k}{(2\pi)^3} \int d^3p b[\epsilon_k^*(p) - \mu_k], \quad (34)$$

and

$$\bar{n}_k = \frac{d_k}{(2\pi)^3} \int d^3p b[\bar{\epsilon}_k^*(p) + \mu_k], \quad (35)$$

respectively, where $d_k = 1$ is the spin degeneracy for K . The Bose-Einstein distribution function reads

$$b[x] = \frac{1}{(e^{x/T} - 1)}. \quad (36)$$

When the condition for kaon condensation (KC)[21, 22] is not satisfied, see Eq.(52) below, the kaons will not condensate and the density of the kaon condensate $n_{\text{KC}} = 0$. In this case the chemical potentials μ_B , μ_S and μ_Q are determined from n_B , n_S^{Total} and n_Q^{Total} . However, when the condition for the kaon condensation $\mu_K = \epsilon_K^*(0)$ is satisfied for either kaon species K^+ or K^0 then that species will condensate. Beyond the condensation point, the strange chemical potential saturates at the threshold energy for the ground states $\mu_K \equiv \epsilon_K^*(0)$. On the other hand if the condition $\mu_K = -\bar{\epsilon}_K^*(0)$ is satisfied for either K^- or \bar{K}^0 antikaon, then either K^- or \bar{K}^0 antikaon will condensate. Beyond the condensation point, the strange

chemical potential saturates at the threshold energy for the ground states $\mu_K \equiv -\bar{\epsilon}_K^*(0)$. We shall return to the kaon condensation when we reach Eq.(52).

The baryon density reads,

$$n_B = \sum_i^{\text{Bs}} B_i [n_i - \bar{n}_i]. \quad (37)$$

The total strangeness density is given by

$$n_S = n_S^{\text{Bs}} + n_S^{\text{Ks}}, \quad (38)$$

where $n_S^{\text{Bs}} = \sum_i^{\text{Bs}} S_i [n_i - \bar{n}_i]$ and $n_S^{\text{Ks}} = \sum_k^{\text{Ks}} S_k [n_k - \bar{n}_k] + S_K n_{\text{KC}}$. The total isospin charge density is given by

$$n_Q = n_Q^{\text{Bs}} + n_Q^{\text{Ks}}, \quad (39)$$

where $n_Q^{\text{Bs}} = \sum_i^{\text{Bs}} Q_i [n_i - \bar{n}_i]$ and $n_Q^{\text{Ks}} = \sum_k^{\text{Ks}} Q_k [n_k - \bar{n}_k] + Q_K n_{\text{KC}}$.

The vector mean fields ω , ϕ and ρ are determined, respectively, as follows

$$\omega = \sum_i^{\text{Bs}} \frac{g_{i\omega}}{m_\omega^2} [n_i - \bar{n}_i] + \sum_k^{\text{Ks}} \frac{g_{k\omega}}{m_\omega^2} [n_k - \bar{n}_k] + \frac{g_{K\omega}}{m_\omega^2} n_{\text{KC}}, \quad (40)$$

$$\phi = \sum_i^{\text{Bs}} \frac{g_{i\phi}}{m_\phi^2} [n_i - \bar{n}_i] + \sum_k^{\text{Ks}} \frac{g_{k\phi}}{m_\phi^2} [n_k - \bar{n}_k] + \frac{g_{K\phi}}{m_\phi^2} n_{\text{KC}}, \quad (41)$$

$$\rho = \sum_i^{\text{Bs}} \frac{g_{i\rho}}{m_\rho^2} I_{3i} [n_i - \bar{n}_i] + \sum_k^{\text{Ks}} \frac{g_{k\rho}}{m_\rho^2} I_{3k} [n_k - \bar{n}_k] + \frac{g_{K\rho}}{m_\rho^2} I_{3k} n_{\text{KC}}. \quad (42)$$

The $g_{i\omega}$, $g_{i\phi}$ and $g_{i\rho}$ are the meson-baryon coupling constants while $g_{k\omega}$, $g_{k\phi}$ and $g_{k\rho}$ are the meson-kaon coupling constants and are determined from the data.

The pressure for hot and dense strange matter is equal to the negative of the grand thermodynamic potential density and is given by

$$P = \frac{1}{3} \sum_i^{\text{Bs}} \frac{d_i}{(2\pi)^3} \int d^3 p \frac{p^2}{\epsilon_i^*} \left(f[\epsilon_i^*(p) - \mu_i] + f[\bar{\epsilon}_i^*(p) + \mu_i] \right) + P_K + \frac{1}{2} m_\omega^2 \omega^2 + \frac{1}{2} m_\phi^2 \phi^2 + \frac{1}{2} m_\rho^2 \rho^2 - \frac{1}{2} m_\sigma^2 \sigma^2 - \frac{1}{2} m_{\sigma^*}^2 \sigma^{*2}, \quad (43)$$

where summation i runs over the 8 species of the baryon octet $p, n, \Lambda, \Sigma^+, \Sigma^0, \Sigma^-$ and Ξ^0, Ξ^- .

The thermal kaon pressure is given by

$$P_K = \frac{1}{3} \sum_k^{\text{Ks}} \frac{d_k}{(2\pi)^3} \int d^3 k \frac{k^2}{\sqrt{k^2 + M_k^{*2}}} \left(b[\epsilon_k^*(k) - \mu_k] + b[\bar{\epsilon}_k^*(k) + \mu_k] \right), \quad (44)$$

where the summation k run over the kaon doublet species K^+, K^0 .

The scalar mean fields σ and σ^* are calculated by maximizing the pressure

$$\frac{\partial P}{\partial \sigma} = 0, \quad (45)$$

$$\frac{\partial P}{\partial \sigma^*} = 0. \quad (46)$$

The pressure depends explicitly on the scalar mean fields σ, σ^* through the last two terms in Eq.(43). It also depends on the baryon and kaon effective masses M_i^* and M_k^* which in turn depend on σ and σ^* . If we write the pressure as a function of $(\{M_i^*\}, \{M_k^*\})$ and (σ, σ^*) , the extremization of $P(\{M_i^*\}, \{M_k^*\}, \sigma, \sigma^*)$ with respect to the scalar fields σ and σ^* can be written as

$$\frac{\partial P}{\partial \sigma} = \sum_i \left(\frac{\partial P}{\partial M_i^*} \right)_{\{M_j\}_{j \neq i}, \mu_B, \mu_S, \mu_Q, T} \frac{\partial M_i^*}{\partial \sigma} + \left(\frac{\partial P}{\partial \sigma} \right)_{\{M_j\}} = 0. \quad (47)$$

A similar expression can be written for $\frac{\partial P}{\partial \sigma^*} = 0$. The coupling of the scalar mean fields σ, σ^* with the quarks in the non-overlapping MIT bags through the solution of the point-like Dirac equation should be taken into account to satisfy the self-consistency condition. This constraint is essential to obtain the correct solution of the scalar mean field σ, σ^* .

The pressure of the condensate kaon P_{KC} , if it exists, contributes to the total pressure of the hot and dense strange hadronic matter. The total pressure of the system becomes

$$P^{\text{total}} = P + P_{\text{KC}}. \quad (48)$$

The contribution of the kaon condensate pressure reads [23, 24]

$$P_{\text{KC}} = \frac{1}{2} (f\theta)^2 [\epsilon_k^*(0) - \mu_k] [\bar{\epsilon}_k^*(0) + \mu_k], \quad (49)$$

where

$$\epsilon_k^*(0) = M_k^* + X_k \quad (50)$$

$$\bar{\epsilon}_k^*(0) = M_k^* - X_k. \quad (51)$$

This equation is derived by assuming that the kaon amplitude is replaced by the ansatz $K = f\theta/\sqrt{2}$ and $K\bar{K} = \frac{1}{2}f^2\theta^2$ where f is the kaon decay constant and θ is the dimensionless kaon field strength. The variation of Equation (49) gives

$$\delta P_{\text{KC}} = f^2\theta [\epsilon_k^*(0) - \mu_k] [\bar{\epsilon}_k^*(0) + \mu_k] = 0. \quad (52)$$

There are three solutions to Eq.(52) that determine the conditions for kaon condensation. The trivial solution is that kaon amplitude vanishes $\theta = 0$. This case means that no kaon condensation takes place in the system and subsequently $n_{\text{KC}} = 0$. The other two solutions are determined as follows: if $[\epsilon_k^*(0) - \mu_k] = 0$ either $k = (K^+ \text{ or } K^0)$ will condensate, and if $[\bar{\epsilon}_k^*(0) + \mu_k] = 0$ either antikaon $k = (K^- \text{ or } \bar{K}^0)$ will condensate. The density of the kaon condensate is given by,

$$n_{\text{KC}} = (f\theta)^2 (\mu_k - X_k). \quad (53)$$

In this case, the charge chemical potential becomes $\mu_Q(\epsilon_K^*(0), \mu_S)$ for either K^+ or K^0 condensate or $\mu_Q(-\bar{\epsilon}_K^*(0), \mu_S)$ for either K^- or \bar{K}^0 condensate since $\mu_K = S_K \mu_S + Q_K \mu_Q$ and n_S^{Total} is conserved. It is interesting to note here that the three solutions give $P_{\text{KC}} = 0$ and normally the pressure of the condensate kaons contributes indirectly in the strange hadrons abundances and the total energy density of the system.

III. FITTING PARAMETERS FOR YY POTENTIALS

We assume that the σ and ω mesons couple only to the up and down quarks while σ^* and ϕ couple to the strange quark. We thus set $g_{r\phi} = g_{r\sigma^*} = g_{s\sigma} = g_{s\omega} = 0$ and $g_{s\rho} = 0$ where r refers to the up and down flavors while s denotes the strange flavor. By assuming the $SU(6)$ symmetry of the simple quark model we have the relations $g_{s\sigma^*} = \sqrt{2}g_{r\sigma}$ and $g_{s\phi} = -\sqrt{2}g_{r\omega}$. The σ mean field is supposed to simulate the exchange of correlated pairs of pions and may represent a very broad resonance observed in $\pi\pi$ scattering. We take $m_\sigma = 550$ MeV. The vector ω and ρ mesons are identified with the actual mesons whose masses are $m_\omega = 783$ MeV and $m_\rho = 770$ MeV, respectively. Since the mean fields, σ and ω , are considered as $\langle u\bar{d} \rangle$ condensates, they interact only with u, d -quark in the baryons and kaons. On the other hand, the scalar and vector mean fields σ^*, ϕ are considered as $\langle s\bar{s} \rangle$ condensates and interact only with the s -quarks in the baryons and kaons. The isovector mean fields interact with the u, d -quarks in baryons and kaons.

The coupling of each baryon species with the vector mesons is calculated by counting the constituent quarks

$$g_{i\omega} = \sum_q^3 g_{q\omega} = \sum_r g_{r\omega}, \quad (54)$$

and

$$g_{i\phi} = \sum_q^3 g_{q\phi} = \sum_s g_{s\phi}, \quad (55)$$

while

$$g_{i\rho} = g_{q\rho}. \quad (56)$$

With these assumptions the only free parameters left at our disposal are the quark-meson coupling constants $g_{r\sigma}$ and $g_{r\omega}$ and the bag coupling constants $g_{i\sigma}^{\text{bag}}, g_{i\sigma^*}^{\text{bag}}$ for the 4 baryon species and these parameters are adjusted to fit nuclear properties as well as the extrapolated properties of hypernuclear matter. The coupling constants of the scalar and vector mesons to the nonstrange quarks are taken as $g_{r\sigma} = 1$ and $g_{r\omega} = 2.705$ which together with a bag coupling constant $g_{N\sigma}^{\text{bag}} = 6.81$ yield a binding energy of 16 MeV and a compressibility K_V^{-1} of 289 MeV at the normal saturation density $\rho_0 = 0.17\text{fm}^{-3}$ of nuclear matter[2, 5, 6]. The isospin vector meson coupling constant for ρ -meson is taken $g_{q\rho} = 8.086$ to reproduce the bulk symmetry energy. The coupling constants $g_{i\sigma}^{\text{bag}}$ and $g_{i\sigma^*}^{\text{bag}}$ where $i = \Lambda, \Sigma, \Xi$ are determined from the YY potentials assumptions. In the present calculation, we have considered two different models for the hyperon-hyperon interactions.

Model (I) is designed to mimic the consequences of the Nijmegen hard-core potential model D [11, 12, 14]. It is nevertheless constrained by Λ and Ξ nuclear phenomenology, and by a few $\Lambda\Lambda$ hypernuclei reported to date. It accounts more realistically for the attractive $\Lambda\Lambda$ and $N\Xi$ interactions, but ignores altogether Σ hyperons.

Model (II) is designed to generate qualitatively similar baryon potentials to those obtained in the BHF approximation from the SU(3) extensions of the Nijmegen soft-core potential model NSC97[15, 16, 17, 18]. The phenomenology in this model departs substantially from that in Model I. The NSC97 model has been tuned up to reproduce certain characteristics of Λ hypernuclei, particularly its version NSC97f. It yields particularly attractive $\Xi\Xi$, $\Sigma\Sigma$ and $\Sigma\Xi$ interactions. Some of the shortcomings of this model are the vanishingly weak $\Lambda\Lambda$ and $N\Xi$ interactions which are in contradiction with the little experimental evidence available from $\Lambda\Lambda$ hypernuclei and from Ξ -nucleus interaction. The coupling constant $g_{K\sigma}^{\text{bag}}$ is determined to fit the kaon potentials embedded in nuclear matter $U_{K^+}^{(N)} = 20$ MeV and $U_{K^-}^{(N)} = -120$ to -180 MeV. This potential can be fitted when we redefine $g_{K\omega} = 1.7g_{q\omega}$ and $g_{K\sigma}^{\text{bag}} = 2.27$ keeping in the mind that we have taken $g_{K\sigma^*}^{\text{bag}} = \sqrt{2}g_{K\sigma}^{\text{bag}}$. In our calculation we

shall adopt $g_{K\omega} = g_{q\omega}$ as the normal case and we shall consider the case $g_{K\omega} = 1.7g_{q\omega}$ as a special case.

Table I summarizes the values used in the current work for the basic quark-meson coupling constants as well as the two sets of the constants $g_{i\sigma}^{\text{bag}}$ and $g_{i\sigma^*}^{\text{bag}}$ in the bag parameter $B_i(\sigma, \sigma^*)$. These sets are chosen to fit nuclear and hypernuclear properties. The parameters $g_{i\sigma}^{\text{bag}}$ are taken to fit the hyperon potentials in nuclear matter[11]:

$$\begin{aligned} U_{\Lambda}^{(N)}(\rho_0) &= -30 \text{ MeV}, \\ U_{\Sigma}^{(N)}(\rho_0) &= +30 \text{ MeV}, \\ U_{\Xi}^{(N)}(\rho_0) &= -18 \text{ MeV}, \end{aligned} \tag{57}$$

where the hyperon potentials are defined by

$$U_i^{(i)} = (M_i^* - M_i) + (g_{i\omega}\omega + g_{i\phi}\phi). \tag{58}$$

However, we make two different choices for the constants $g_{i\sigma^*}^{\text{bag}}$.

In the first set, Model I, the medium constants $g_{i\sigma^*}^{\text{bag}}$ are adjusted so that the potential of a single hyperon embedded in a bath of Ξ matter becomes

$$U_{\Xi}^{\Xi}(\rho_0) = U_{\Lambda}^{\Xi}(\rho_0) = -40 \text{ MeV} \tag{59}$$

in accordance with the attractive hyperon-hyperon interaction of the Nijmegen hard core potential Model D[11, 13]. Furthermore, we adopt the approximation $U_{\Xi}^{\Xi}(\rho_0) \approx U_{\Sigma}^{\Xi}(\rho_0)$ to fit the medium constants. The resulting $U_{\Lambda}^{(\Lambda)}(\rho_0/2)$ is about -20 MeV.

In Model II, we have adjusted the bag constants $g_{i\sigma^*}^{\text{bag}}$ where $i = \Lambda, \Sigma, \Xi$ to reproduce qualitatively the same binding energy curves of each hyperon species in its own hyperonic matter B_i^i as those produced by the Model NSC97f[17, 19]. No binding occurs for Λ hyperons. On the other hand, Σ matter is deeply bound at -33 MeV per baryon at $\rho_{\Sigma 0}$ which is twice as deep as ordinary nuclear matter, and Ξ matter has an energy of -23 MeV per baryon at $\rho_{\Xi 0}$.

IV. DISCUSSIONS AND CONCLUSIONS

We have studied the hadronic matter with the conserved strangeness density $n_S = 0$ at finite temperature using the modified quark meson coupling model (MQMC) which takes into

account the quarks degree of freedom confined in the bag as well as the medium dependence of the bag constant B . We have chosen a direct coupling of the bag parameter B to the scalar mean fields σ and σ^* and the bag parameter becomes $B \equiv B(\sigma, \sigma^*)$. The quarks and anti-quarks confined in the hadrons are coupled to the scalar mean fields σ and σ^* and the vector mean fields ω and ϕ and isovector mean field ρ . At first, we have studied the symmetric hot and dense strange hadronic system of baryons and kaons with a neutral isospin charge $n_Q/n_B = 0$ and with a conserved zero net strangeness $n_S = 0$. Then, we have considered the asymmetric system with a conserved isospin charge fraction n_Q/n_B and a conserved zero net strangeness. This is relevant for heavy-ions collision where it is possible to have an asymmetry system with a conserved low isospin charge fraction. A special attention is given for the conserved low isospin charge fraction $n_Q/n_B = 0.0$ to -0.2 .

In our calculation we have used two slightly different versions of Model I. In the fitting potential set (Ia) we have taken $g_{K\omega} = g_{q\omega}$ based on the simple $SU(6)$ symmetry while in the fitting potential set (Ib) we have taken $g_{K\omega} = 1.7g_{q\omega}$ in order to fit the kaon potential depths $U_{K^-}^{(N)}$ and $U_{K^+}^{(N)}$ for a kaon embedded in the nuclear matter. In Model II, we have adopted $g_{K\omega} = g_{q\omega}$ based on simple $SU(6)$ symmetry.

The chemical potentials μ_B, μ_S and μ_Q are determined using the baryon, strange and isospin-charge densities given by Eqs.(37), (38) and (39), respectively. The vector mean-fields ω and ϕ and the isovector mean field ρ are computed from Eqs.(40), (41) and (42), respectively. Once the values for the chemical potentials (μ_B, μ_S, μ_Q) are given, the values for the scalar mean fields σ and σ^* are calculated by maximizing the pressure using Eqs.(45) and (46), respectively. These constraints should take into account the coupling of the quark with the scalar mean fields in the frame of the point-like Dirac equation exactly[1, 2, 3] to obtain consistent results.

The pressure is given in terms of the effective baryon masses $\{M_i^*\}$ those depend on the bag radii R_i and the scalar mean fields σ and σ^* . For given values of the scalar fields σ, σ^* and vector fields ω, ϕ and ρ , the bag radius for each hadron species i, k is obtained by minimizing the hadron mass with respect to its bag radius using the condition Eq. (14). The pressure is evaluated for specific values of temperature T and chemical potentials (μ_B, μ_S, μ_Q) which in turn become input parameters. The values for σ and σ^* are determined using the extremization conditions given in Eqs.(45) and (46). These constraints take into account the coupling of the constituent quark with the scalar mean fields σ, σ^* in the framework of

the point-like Dirac equation exactly[1, 2, 3].

In Figs.(1),(2),(3),(4),(5) and (6), we display the results using the fitting potential set (Ia). Furthermore, in Figs.(7),(8) and (9), we have studied the effects of kaon potential depths using fitting potential sets (Ia) and (Ib). On the other hand, we have compared the fitting potential sets (Ia) and (II) for Nijmegen hard-core and Nijmegen soft-core potentials, respectively. We have displayed the comparison in Figs.(10) and (11).

In Fig.(1), we display the density fraction for each baryon species $x_i = (n_i - \bar{n}_i)/n_B$ versus the baryonic density n_B with several temperatures. The strange hadrons appear in the system at rather low temperatures $T \approx 80$ MeV and then they are produced abundantly when the temperature increases $T > 100$ MeV. However, the abundance of Σ seems to be higher than Λ because it has a higher multiplicity factor. On the other hand, the abundance of Ξ is the lowest. Moreover, the production of strange baryons seems to be modified crucially at temperatures above the critical temperature $T = 170$ MeV. The phase transition from the hadronic phase to the quark-gluon-plasma (QGP) phase is believed to take place at this critical temperature.

In Fig.(2), we display the abundance ratio for the anti-baryon over the baryon for each baryon species \bar{n}_i/n_i with several temperatures. It is seen that for temperature $T < 120$ MeV the production of the anti-baryons is negligible. However, when the temperature increases $T \geq 150$ MeV, the anti-baryons are produced significantly in the system. Furthermore, we have seen that the ratio of the anti-baryon abundance over baryon abundance for strange baryon species, \bar{n}_i/n_i , is relatively large in particular for small baryon density n_B . This ratio seems to increase with the baryon strangeness number as follows:

$$\frac{\bar{\Xi}}{\Xi} > \frac{\bar{\Lambda}}{\Lambda}, \frac{\bar{\Sigma}}{\Sigma} > \frac{\bar{N}}{N}. \quad (60)$$

The enhancement of anti-hyperon abundance ratio over the antiproton abundance ratio in the relativistic nuclear collisions has been observed earlier[25]. Furthermore, the anti-baryon production increases significantly with the temperature in particular when the temperature reaches the critical one.

We display the kaon production at finite temperature in Fig.(3). In Fig.(3.a), we show the ratio of anti-kaon abundance over kaon abundance versus the baryon density n_B with various temperatures while the net kaon density fraction $x_K = (n_K - \bar{n}_K)/n_B$ versus baryon density n_B at various temperatures is displayed in Fig.(3.b). The kaon and anti-kaon production

in the system increases as the temperature increases especially for temperatures exceeding $T \approx 100$ MeV. We see that a large mesonic strangeness $n_S^K > 0.2$ can be reached at temperature $T = 170$ MeV when kaons are produced abundantly in the system. The ideal gas approximation without any interaction always gives underestimated results for anti-hadron abundance over hadron abundance than the MQMC results. The MQMC enhances the antiparticle/particle ratios.

The possibility of kaon condensation in the heavy ions collision is a crucial issue. This implies that the equation of states will be softer and more strange baryons and kaons will accumulate in the system. Indeed, it is shown that kaon condensation plays a significant role in the physics of neutron stars[26]. One of the major themes of the present work is to study the possibility of the onset of kaon condensation in heavy-ion collision physics. The necessary condition for the onset of kaon condensation is to satisfy Eq.(52). This equation has three solutions. The first (trivial) solution is that the kaon amplitude vanishes $\theta = 0$ and the kaons do not condensate in the system. The other two nontrivial solutions raise the possibility that the kaons condense smoothly in the system. The onset for kaon K^0 or K^+ condensation is only possible when

$$\mu_k = \epsilon_k^*(0) \quad (61)$$

while the onset of antikaon \bar{K}^0 or K^- condensation is only possible when

$$\mu_k = -\bar{\epsilon}_k^*(0). \quad (62)$$

When the condition for the onset of kaon condensation is satisfied, the kaons start to condense smoothly and the strange chemical potential is evaluated either from Eq.(61) or (62). After the kaon condensation takes place in the system the strange chemical potential μ_S becomes an input parameter and the amplitude of the kaon condensation is calculated by conserving the total strangeness of the system. The density contribution of the kaon condensate to the total density of the system is calculated using Eq.(53). In the present work, we have tested the kaon condensation possibility. In Fig.(4), we display the kaon chemical potential μ_K and the kaon threshold effective energy $\epsilon_k^*(0)$ versus the baryonic density n_B with various temperatures. The isospin charge chemical potential μ_Q vanishes for the symmetric strange hadronic system. We have displayed $\mu_K = \mu_S(\mu_Q = 0)$ where μ_S and μ_Q are the strange and charge chemical potentials respectively. The kaon chemical potential μ_K is

found always less than the kaon threshold energy $\epsilon_k^*(0)$ for the all baryon densities n_B . This indicates that the kaons do not condensate at all and they are only produced thermally in the system. Therefore, the kaon condensation does not take place at any temperature and density in the heavy-ions collision experiments where the total strangeness is conserved to zero for a system that consists baryons and kaons. However, the situation is completely different in neutron stars where there is an enough time for the conservation of strangeness to be violated by the weak interaction[26].

In Figs.(5) and (6), we display the hadron effective masses versus the baryon density n_B for baryons and kaons. The effective hadron masses do not vanish at large baryon densities in the context of MQMC model unlike the standard Walecka model where the effective hadronic masses tend to vanish at large baryon density. The realistic case of effectively massive hadrons is actually a characteristic result for the MQMC model. Indeed, in the hadronic phase, the hadron effective masses should not vanish until chiral symmetry is restored or the QGP phase transition takes place. At the point of the phase transition, there is a sharp drop in the hadron effective masses and all the hadrons in the system will dissolve into their constituent quarks. Furthermore, the quarks attain their current masses which are very small for the up and down flavors. At this point, however, bubbles of the QGP are formed in the system. Therefore, we do not find it appropriate, in the realistic situation relevant to heavy-ion collisions, to extrapolate the study of the onset of kaon condensation to massless hadrons since these massless hadrons exist only at the point of the phase transition.

The fitting parameters extracted from the nuclear potential depths play an important role in phenomenological studies and their results and conclusions. This is particularly true for the properties of the kaons embedded in nuclear matter. We have considered the potential fitting set (Ib) where the vector coupling for the kaon is fitted using kaon potential depths to reproduce $U_{K^-}^{(N)}$ and $U_{K^+}^{(N)}$. The other fitting parameters in the fitting potential set (Ib) are exactly the same as those for the potential fitting set (Ia) which produces the Nijmegen hard-core potential depths for the strange baryons. The only difference is that we set $g_{K\omega} = 1.7g_{q\omega}$ to reproduce the kaon potential depths in the fitting potential set (Ib) instead of $g_{K\omega} = g_{q\omega}$, which is based on simple SU(6) counting symmetry, in the fitting potential set (Ia). However, it has been pointed out that $U_{K^-}^{(N)} = -60, -50$ MeV at momentum zero and $T = 0$ fits kaonic data[27]. Indeed, this potential will not affect so much is in the

results of the present work.

We have compared the potential fitting sets (Ia) and (Ib) in Figs.(7),(8) and (9). We see that the modification of the kaon vector coupling does not change the results in a detectable manner except only at rather high temperatures beyond the critical temperature. At $T = 200$ MeV, which is much higher than the critical one, the fitting potential set (Ia) produces slightly more kaons than the set (Ib) since the vector coupling for kaons in the set (Ib) is stronger than that in the set (Ia). In the rest of our calculations, we shall adopt the simple $SU(6)$ symmetry to fit the coupling constant for kaons.

Furthermore we have adopted another set of fitting parameters, set(II), based on $SU(3)$ extensions of the Nijmegen soft-core potential model NSC97. The model yields particularly attractive $\Xi\Xi$, $\Sigma\Sigma$ and $\Xi\Sigma$ interactions. The phenomenology in this model departs substantially from that in the fitting potential fit set (Ia) for large baryonic and strangeness densities where the phase transition to $\Sigma\Sigma$ takes place[8, 19]. In Figs.(10) and (11), we compare the baryon and kaon abundances obtained using the fitting potential sets (Ia) and (II). We see that at high temperature when the strange hadrons are produced, Λ -hadron abundance with the set (Ia) is slightly more than that with the set (II) while the Σ -hadron abundance in the set (Ia) is less than that in the set (II). Nevertheless, we do not see any noticeable change in nucleon and cascade production properties. Furthermore, there is not much difference in total strange baryon production. Similarly, Fig.(11) shows little difference in the kaon production between the fitting potential fits (Ia) and (II).

We have extended our study to hot and dense asymmetric strange hadronic matter. We have considered a system of baryons and kaons with a conserved total zero strangeness $n_S/n_B = 0$ and a conserved finite negative isospin charge density fraction $n_Q/n_B \leq 0$. Generally speaking, the negative value of the isospin charge density fraction n_Q/n_B means that the number of neutrons is more than the number of protons (i.e. $n_n/n_B > n_p/n_B$) in the initial condition of the colliding heavy ions. This is a realistic case in the relativistic heavy-ions collision. The results for the asymmetric system with a conserved negative isospin charge density fraction ($n_Q/n_B < 0$) and a conserved zero net strangeness using the fitting potential set (Ia) are shown in Figs.(12),(13),(14),(15),(16),(17) and (18). The results for $n_Q/n_B = -0.10$ are shown in figures (12),(13) and (14) while the results for $n_Q/n_B = -0.20$ are shown in Figs.(15),(16) and (17). The resulting kaon abundances versus the baryonic density n_B are shown in fig.(18) for several values of $n_Q/n_B = -0.10, -0.20, -0.30$

at temperature $T = 170$ MeV.

The results for asymmetric nuclear matter with several values of isospin charge n_Q/n_B versus temperature using the fitting potential set (Ia) are displayed in Figs.(19) and (20) for a small baryonic density $\rho_B = 0.05\text{fm}^{-3}$. This rather small baryonic density is accessible in RHIC and has a special interest at high temperature in particular in order to study the freezeout chemical potential.

The chemical potential at freezeout is found to be small $\mu_B \approx 46 \pm 5$ MeV at temperature $T \approx 174 \pm 7$ MeV [28, 29]. The substantial decrease of the baryon chemical potential from $\mu_B \approx 270$ MeV at SPS to $\mu_B \approx 45$ MeV at RHIC shows that at mid-rapidity, we are dealing with a low net baryon density in the medium[28]. In our model, the baryon chemical potential $\mu_B \approx 50$ MeV for the critical temperature $T \approx 170$ MeV corresponds the small baryonic density $n_B \approx 0.015\text{fm}^{-3}$. We display the baryon and strange chemical potentials versus the baryonic density n_B at temperature $T = 170$ MeV for the symmetrical nuclear matter in Fig.(21). Other models, however, may lead to higher values for the baryonic density for the chemical freezeout potential[29]. Nonetheless, we shall refer to this small baryon density $n_B \approx 0.05\text{fm}^{-3}$ when we speak about RHIC physics. The Figs.(19) and (20) display kaon abundances for the baryonic density $\rho_B = 0.05\text{fm}^{-3}$.

In Fig.(12), we display the density fraction for each baryon species $x_i = (n_i - \bar{n}_i)/n_B$ versus the baryon density n_B with several temperatures for $n_Q/n_B = -0.1$. The strange hadrons appear at temperatures $T \approx 100$ MeV. The strange baryon species abundance increases significantly at higher temperatures. Moreover, the differences in the abundance of different charge states of baryon species Σ^- , Σ^0 , Σ^+ and Ξ^0 , Ξ^+ are small at low temperatures but they increase when the temperature increases. At higher temperature, the baryon species Σ^- , Σ^0 , Σ^+ play more important role to conserve the isospin charge density n_Q/n_B . These results become more evident when the value of the negative charge density fraction n_Q/n_B is increased. The results for $n_Q/n_B = -0.2$ are displayed in Fig.(15). It is seen that the abundance for net proton density fraction attends to saturate to some value in particular when the negative isospin charge density fraction (the absolute value!) becomes rather large ($n_Q/n_B = -0.2$, $n_p/n_B \approx 0.30$) while the density fraction for neutrons increases with the temperature. However, the conserved isospin charge density fraction is preserved by creating more charged strange hadrons. Furthermore, when the temperature increases and exceeds $T = 100$ MeV, more anti-hadrons are produced in the system.

In Figs.(13) and (16), we display the kaon production and the ratio of anti-kaon abundance over kaon abundance for each kaon species (K^+ , K^0) with several temperatures for $n_Q/n_B = -0.1$ and $n_Q/n_B = -0.2$, respectively. At first, we display the net kaon density fraction $x_K = (n_K - \bar{n}_K)/n_B$ versus the baryonic density n_B with various temperatures in Figs.(13.a,16.a). It is seen that $(n_{K^0} - n_{\bar{K}^0})/n_B$ is much larger than $(n_{K^+} - n_{K^-})/n_B$ in such a system. In Figs.(13.b,16.b), we find that the K^0 is produced more than \bar{K}^0 . The situation is similar for the charged kaons. However, when the asymmetry of the hypernuclear matter is increased, the neutral kaon K^0 is produced more than its antiparticle \bar{K}^0 at high baryonic density n_B and this, however, is not the case for the charged kaon K^+ and its antiparticle K^- . The conservation of the net strangeness for the asymmetric system seems to be preserved by K^0, \bar{K}^0 at high temperatures. Consequently, when the negative isospin charge n_Q/n_B is increased, $(n_{K^0} - n_{\bar{K}^0})/n_B$ becomes more dominant in the system. We have seen also that at high temperature and large baryonic density n_B , the negative kaons K^- are produced more than the K^+ (i.e. $n_{K^-} > n_{K^+}$) for the isospin charge density fraction $n_Q/n_B \geq -0.2$.

We have examined the possibility for the onset of kaon condensation in the asymmetric strange hadrons system. The necessary condition for kaon condensation is satisfied when the kaon threshold energy $\epsilon_k^*(0)$ becomes equal to its chemical potential μ_K . In Figs(14) and (17) we display the kaon chemical potential μ_K and the kaon threshold effective energy $\epsilon_k^*(0)$ versus the baryonic density n_B with various temperatures for $n_Q/n_B = -0.1$ and $n_Q/n_B = -0.2$, respectively. We see that the kaon's threshold energy is always larger than its chemical potential. Their curves are almost parallel to each other at the large baryonic density. Furthermore, when the nuclear matter asymmetry is increased by increasing the negative isospin charge n_Q/n_B to reach the maximal one $n_Q/n_B = -0.5$ (neutron matter), the onset of kaon condensation is not possible even at very large density because the strange chemical potential μ_S in the medium is modified in a manner to avoid the onset of kaon condensation. Our results show that no signature for the onset kaon condensation can exist in the system and the kaons are produced only thermally in the heavy-ions collision.

We have examined the production of K^0 and K^+ and their anti-particles at high temperature for several values of isospin charge density fraction n_Q/n_B . Fig. (18) shows the kaon and antikaon abundances versus baryonic density for three different isospin charge fraction $n_Q/n_B = -0.1, -0.2$ and -0.3 at the temperature $T = 170$ MeV. This temperature is accessible in RHIC energy and has a special interest for the freezeout chemical potential

at relatively small baryonic density. We have seen that both K^0 and K^+ and their anti-particles \bar{K}^0 and K^- are produced abundantly at low baryonic density. The net abundance for $(n_{K^+} - n_{K^-})/n_B$ tends to be almost constant with respect to baryonic density n_B . Furthermore, it decreases when the asymmetry of the system increases by increasing the negative value of the isospin charge density fraction n_Q/n_B . The value for $(n_{K^+} - n_{K^-})/n_B$ becomes negative when the isospin charge density fraction reaches $n_Q/n_B < -0.25$. This means that the number of antikaon K^- exceeds the number of K^+ in the system. However, in the realistic situation, the isospin charge density fraction normally takes the value $n_Q/n_B = 0$ to -0.1 in RHIC. Therefore, the production of K^+ is expected to be more dominant than K^- in RHIC for small isospin charge density fractions. However, it is expected that situation will change drastically for the relatively high asymmetric nuclear matter when the isospin charge density fraction exceeds a definite value $n_Q/n_B < -0.25$. This can be verified experimentally by using different isotopes in the colliding heavy ions. Nonetheless, generally speaking, the production of $(n_{K^+} - n_{K^-})/n_B$ is relatively smaller than $(n_{K^0} - n_{\bar{K}^0})/n_B$. Therefore, the neutral kaons in asymmetrical nuclear matter play a more significant role to conserve the zero net strangeness for the system.

In Fig.(19), the kaon and anti-kaon density fractions versus temperature at the rather small baryonic density $n_B = 0.05(\text{fm}^{-3})$ are displayed. Several values of n_Q/n_B are considered in the calculation. The system with a low baryonic density $n_B = 0.05\text{fm}^{-3}$ and high temperature $T = 170\text{MeV}$ could be produced in RHIC where the phase transition from the hadronic phase to the QGP is expected to take place in the system. It is seen that kaons are produced abundantly when the temperature increases and exceeds $T > 120\text{MeV}$ and this production becomes significant when the temperature reaches $T = 170\text{MeV}$. Furthermore, it is seen that n_{K^0} lies always above $n_{\bar{K}^0}$ but this is not the case for n_{K^+} and n_{K^-} where $(n_{K^+} - n_{K^-})/n_B$ decreases as the asymmetry of the system increases. The net density fraction for the charged kaons $(n_{K^+} - n_{K^-})/n_B$ and neutral kaons $(n_{K^0} - n_{\bar{K}^0})/n_B$ versus temperature are displayed in Fig.(20). We have found that $(n_{K^0} - n_{\bar{K}^0})/n_B > (n_{K^+} - n_{K^-})/n_B$ for asymmetric nuclear matter. This means that K^0 becomes more dominant as the temperature increases and as the isospin charge density fraction n_Q/n_B decreases from -0.1 to -0.4 .

V. SUMMARY

We have studied strange hadronic matter composed of the octet baryons and doublet kaons with a conserved zero total strangeness for baryonic and mesonic hadrons $n_S/n_B = \left(n_S^{\text{Baryons}} + n_S^{\text{Kaons}} \right)/n_B = 0$ and a conserved asymmetric nuclear matter with a finite fraction of the isospin charge density n_Q/n_B . The RHIC physics is reached at rather low baryonic density $n_B \approx 0.05\text{fm}^{-3}$ and high temperature $T \approx 150 - 170 \text{ MeV}$ [28]. We have shown that the strange hadrons, baryons and kaons, are only produced thermally in the system. However, the thermal production of the strange hadrons starts smoothly at rather low temperatures and then they are abundantly produced when the temperature reaches $T \approx 170\text{MeV}$. Indeed, the striking result is that we have not found any evidence for kaon condensation in asymmetric dense nuclear matter even for highly asymmetric system. The kaon threshold energy is always higher than the kaon chemical potential. The kaon chemical potential is given by Eq.(30). We have solved the baryon, strange and isospin chemical potentials μ_B , μ_S and μ_Q , respectively, self-consistently. In warm and hot dense medium, the strange chemical potential μ_S is finite even for a system with the total zero strangeness and it likely modifies itself in a manner to decrease the kaon chemical potential to be always lower than the kaon threshold energy. Therefore, the kaons do not condensate at RHIC energies even for a highly asymmetric and dense nuclear matter. Nonetheless, in the cold dense matter, the strange chemical potential μ_S is normally fixed to zero for a system with a total zero strangeness. In this case, it is possible for the antikaon (kaon) to condensate at very high baryonic density. However, our results show that μ_S can attain a small positive value at large baryonic density n_B at low temperature. This modification in μ_S reduces the possibility for kaon condensation at high n_B . Therefore, the results at finite temperature suggest that μ_S could also attains a small finite value at large n_B in order to maintain the conservation of the total zero strangeness for the cold dense matter. It is interesting to note here that the effective hadronic masses do not vanish in the hadronic phase in our model. The effective hadronic masses attain small values only in the chiral phase transition and the phase transition to the QGP. In the QGP, the hadrons dissolve and disappear and the kaons will not be produced. On the other hand, at very high densities and low temperatures the quark color superconductivity will dominate. The strange hadrons and their anti-particles are normally produced at high temperatures and low baryonic densities which are the ideal

circumstances at the RHIC energies. Furthermore, when the system freezes out, the strange baryons and kaons might survive with a negative net strangeness for the baryonic sector $n_S^{\text{baryons}}/n_B = 0.0$ to -0.25 and with positive net strangeness for the mesonic sector (i.e. kaons) but the total strangeness for the baryonic system and kaons is conserved to zero. However, when the asymmetry of the system is increased by decreasing n_Q/n_B , the K^0 will dominate over \bar{K}^0 . For highly asymmetric nuclear matter (i.e.: $n_Q/n_B < -0.2$) and/or very large baryonic density the K^- becomes more dominant than K^+ . However, the strange hadrons might survive when the system cools down.

Acknowledgments

I. Z. gratefully acknowledges support from the Alexander von Humboldt Foundation. He is also indebted to Dr. F. Arafat, president of Palestine Academy for Science and Technology for his hospitality that made his stay in Gaza possible during 2002-2004. The authors are indebted to Deutsche Forschungsgemeinschaft for the financial support during the early stage of the present project through the grant GR 243/51-1. I. Z. and H. R. J. thank G. Shahin for his assistance in the computational work. I.Z. thanks C. Greiner, J. Schaffner-Bielich, L. Tolos and J-P. Leroy for the discussions and comments.

- [1] K. Saito and A. W. Thomas, Phys. Lett. B **327**, 9 (1994).
- [2] X. Jin and B. K. Jennings, Phys. Rev. C **54**, 1427 (1996).
- [3] X. Jin and B. K. Jennings, Phys. lett. B **374**, 13 (1996).
- [4] H. Mueller and B. K. Jennings, Nucl. Phys. A **626**, 966 (1997).
- [5] I. Zakout and H. R. Jaqaman, Phys. Rev. C **59**, 962 (1999).
- [6] I. Zakout and H. R. Jaqaman, Phys. Rev. C **59**, 968 (1999).
- [7] I. Zakout, H. R. Jaqaman, S. Pal, H. Stöcker, and W. Greiner, Phys. Rev. C **61**, 055208 (2000).
- [8] I. Zakout, H. R. Jaqaman, and W. Greiner, J. Phys. G **27**, 1939 (2001).
- [9] S. Pal, M. Hanauske, I. Zakout, H. Stöcker, and W. Greiner, Phys. Rev. C **60**, 015802 (1999).
- [10] J. Schaffner, C. B. Dover, A. Gal, C. Greiner, and H. Stöcker, Phys. Rev. Lett. **71**, 1328

(1993).

- [11] J. Schaffner, C. B. Dover, A. Gal, C. G. D. J. Millener, and H. Stöcker, *Annals Phys.* **235**, 35 (1994).
- [12] S. Balberg, A. Gal, and J. Schaffner, *Prog. Theor. Phys. Suppl.* **117**, 325 (1994).
- [13] P. Wang, R. K. Su, H. Q. Song, and L. Zhang, *Nucl. Phys. A* **653**, 166 (1999).
- [14] M. Nagels, T. Rijken, and J. de Swart, *Phys. Rev. D* **15**, 2547 (1977).
- [15] T. A. Rijken, V. G. J. Stoks, and Y. Yamamoto, *Phys. Rev. C* **59**, 2140 (1999).
- [16] V. G. J. Stoks and T. A. Rijken, *Phys. Rev. C* **59**, 3009 (1999).
- [17] V. G. J. Stoks and T.-S. H. Lee, *Phys. Rev. C* **60**, 024006 (1999).
- [18] I. Vidana, A. Polls, A. Ramos, M. Hjorth-Jensen, and V. G. J. Stoks, *Phys. Rev. C* **61**, 025802 (2000).
- [19] J. Schaffner-Bielich and A. Gal, *Phys. Rev. C* **62**, 034311 (2000).
- [20] P. K. Panda, A. Mishra, J. M. Eisenberg, and W. Greiner, *Phys. Rev. C* **56**, 3134 (1997).
- [21] D. B. Kaplan and A. E. Nelson, *Phys. Lett. B* **175**, 57 (1986).
- [22] A. E. Nelson and D. B. Kaplan, *Phys. Lett. B* **192**, 193 (1987).
- [23] N. K. Glendenning and J. Schaffner-Bielich, *Phys. Rev. Lett.* **81**, 4564 (1998).
- [24] N. K. Glendenning and J. Schaffner-Bielich, *Phys. Rev. C* **60**, 025803 (1999).
- [25] J. Schaffner, I. N. Mishustin, L. M. Satarov, H. Stocker, and W. Greiner, *Z. Phys. A* **341**, 47 (1991).
- [26] V. Thorsson, M. Prakash, and J. M. Lattimer, *Nucl. Phys. A* **572**, 693 (1994).
- [27] L. Tolos, A. Polls, A. Ramos, and J. Schaffner-Bielich, *Phys. Rev. C* **68**, 024903 (2003).
- [28] P. Braun-Munzinger, D. Magestro, K. Redlich, and J. Stachel, *Phys. Lett. B* **518**, 41 (2001).
- [29] D. Zschiesche, S. Schramm, J. Schaffner-Bielich, H. Stöcker, and W. Greiner, *Phys. Lett. B* **547**, 7 (2002).

Figures

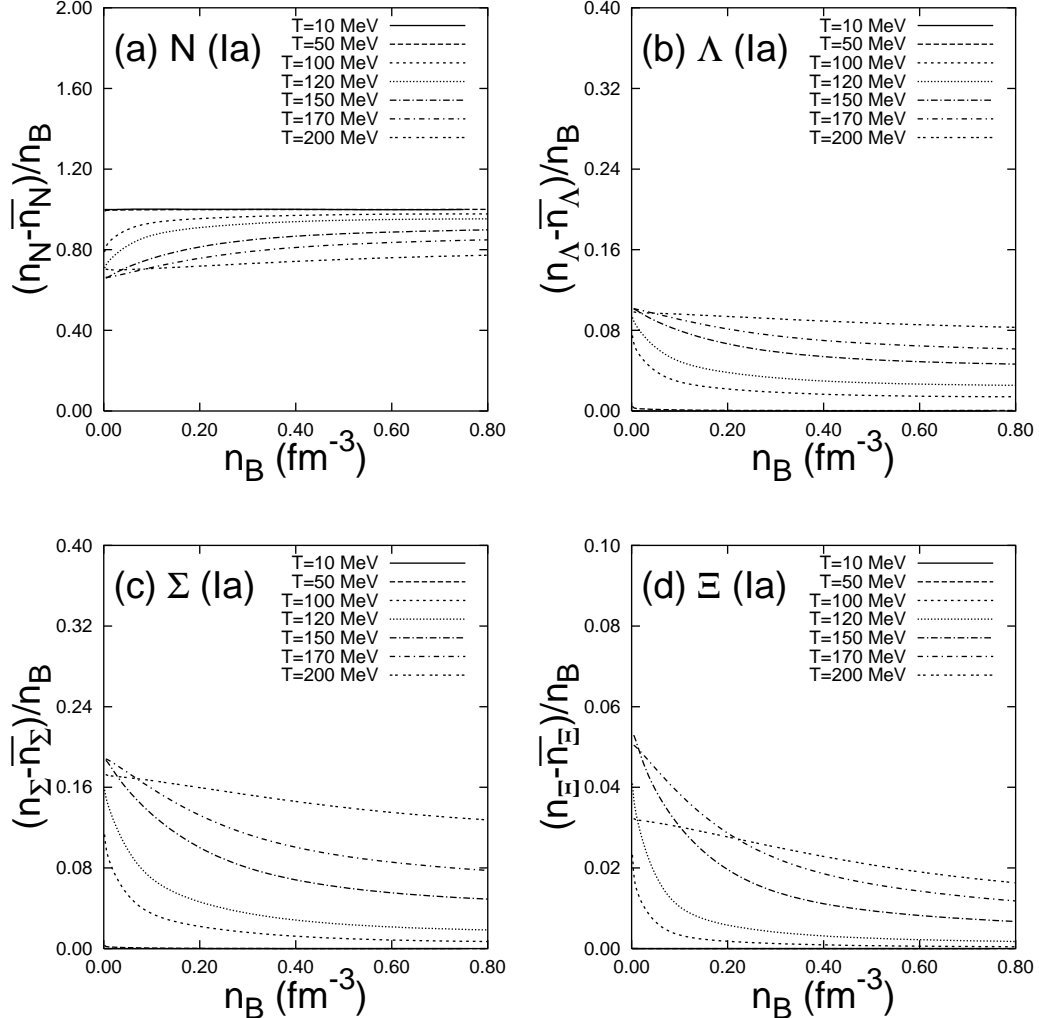


FIG. 1: The density fraction $x_i = (n_i - \bar{n}_i)/n_B$ for baryon species i versus baryon density n_B for several temperatures using the fitting set (Ia). a) N , b) Λ , c) Σ , d) Ξ .

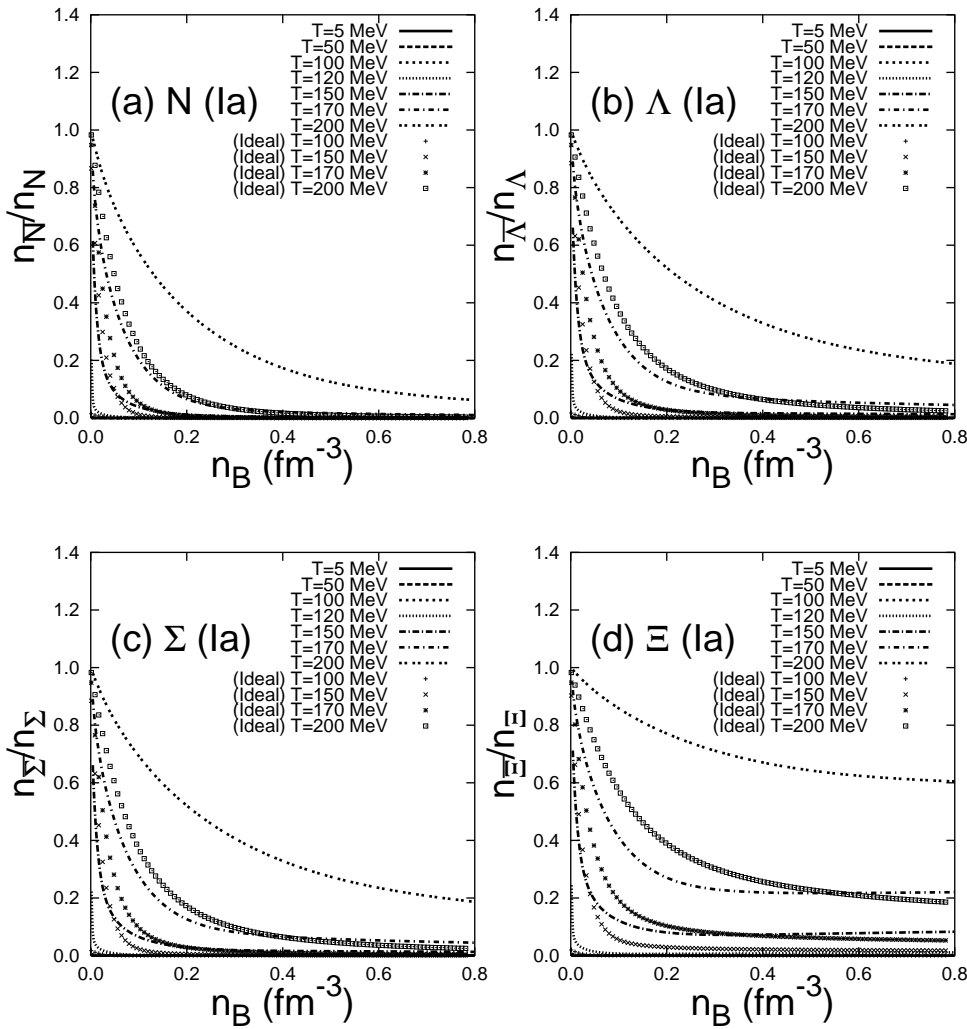


FIG. 2: The ratio of anti-baryon abundance over baryon abundance \bar{n}_i/n_i for each baryon species versus baryon density n_B with several temperatures using the fitting set (Ia). The points correspond to the ideal gas without any interaction. a) N , b) Λ , c) Σ , d) Ξ .

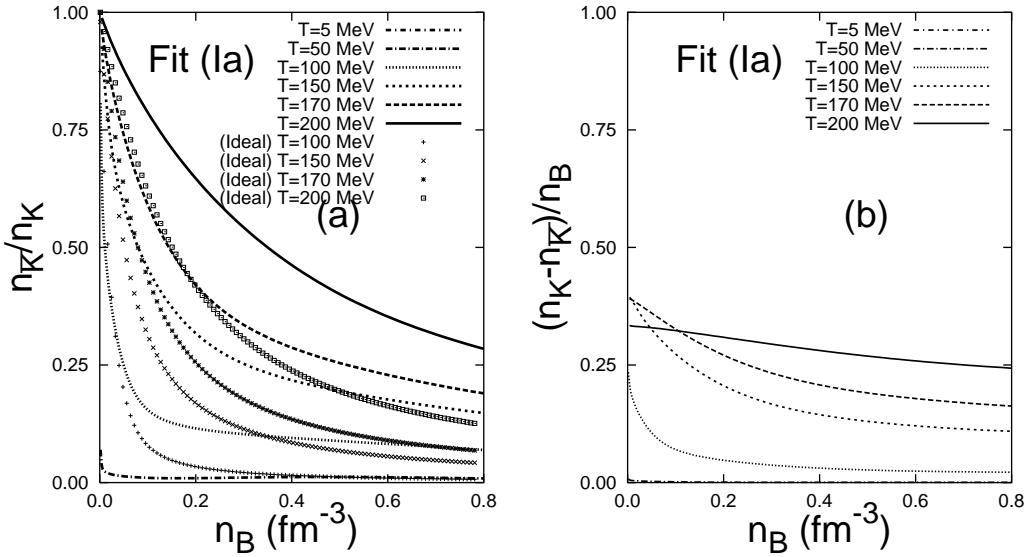


FIG. 3: Kaon abundance vs baryon density n_B for various temperatures using the fitting set (Ia). The points correspond to the ideal gas without any interaction. a) The ratio of anti-kaon abundance over kaon abundance $n_{\bar{K}}/n_K$, b) The kaon density fraction $x_K = (n_K - n_{\bar{K}})/n_B$.

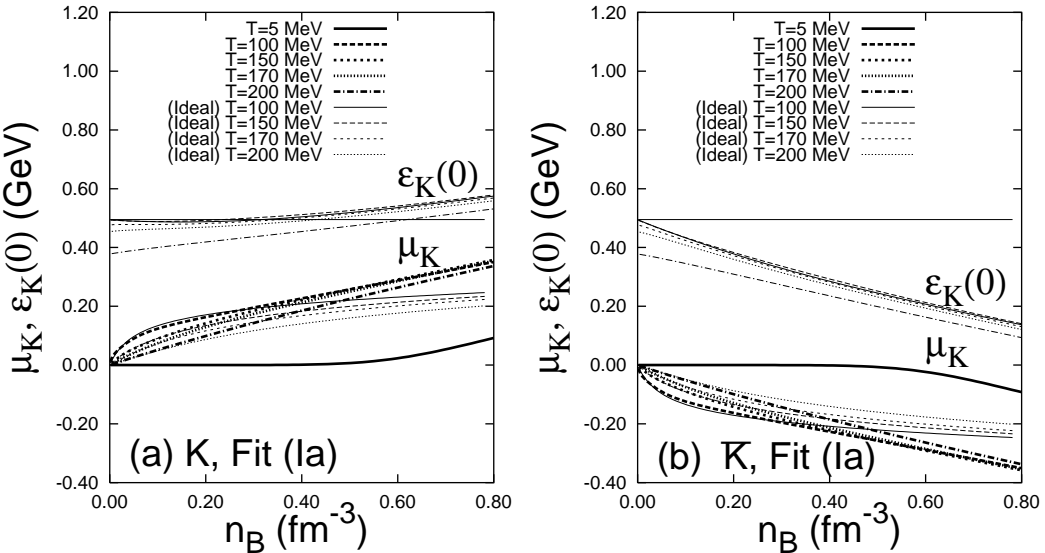


FIG. 4: The strange chemical potential μ_S and the kaon threshold effective energy $\epsilon_K^*(0)$ versus baryon density n_B with various temperatures using the fitting set (Ia). a) Kaons, b) Anti-kaons.

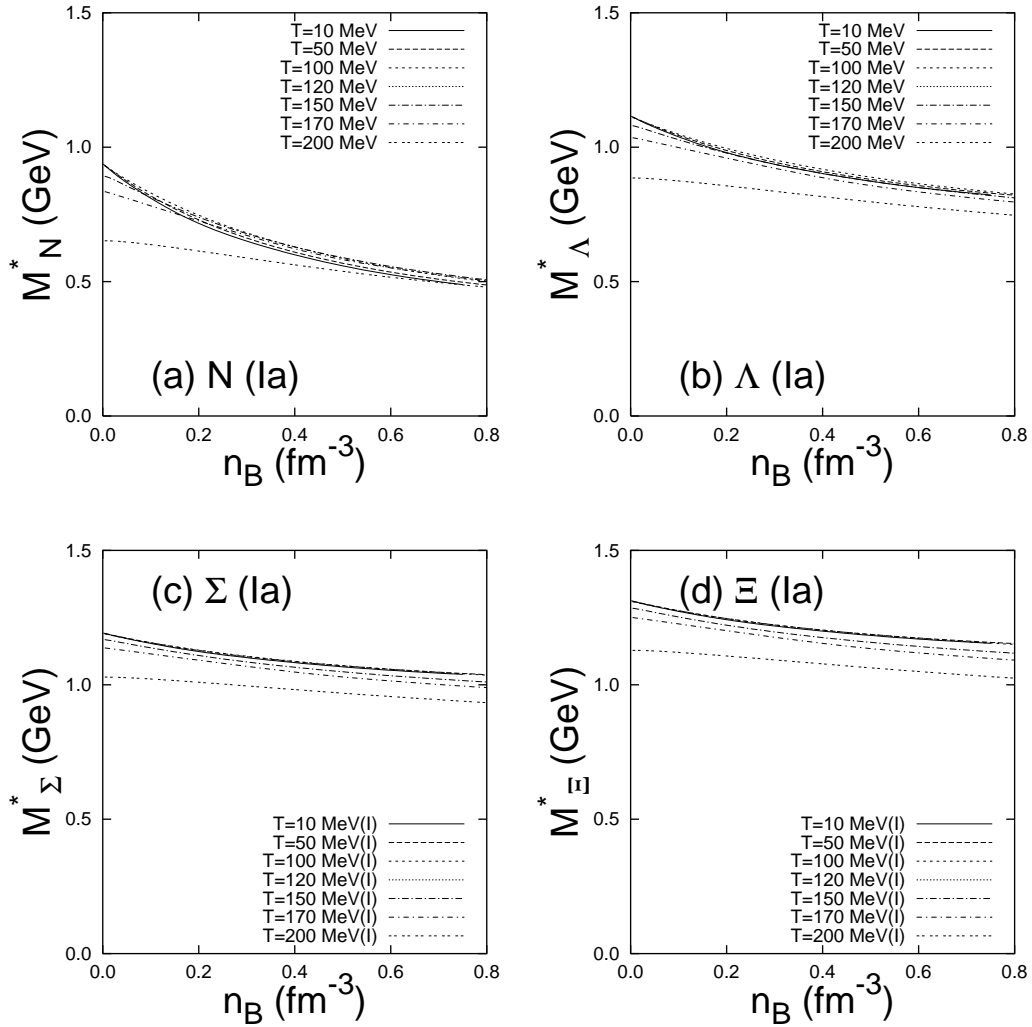


FIG. 5: The effective mass M_i^* for each baryon species versus baryon density n_B with various temperatures using the fitting set (Ia). a) N , b) Λ , c) Σ , d) Ξ .

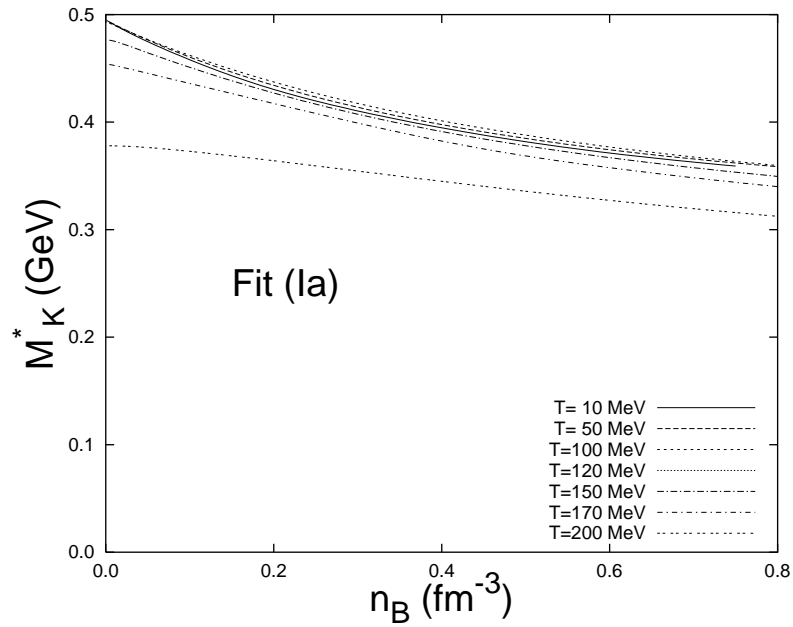


FIG. 6: The effective kaon mass M_K^* versus baryon density n_B for various temperatures using the fitting set (Ia).

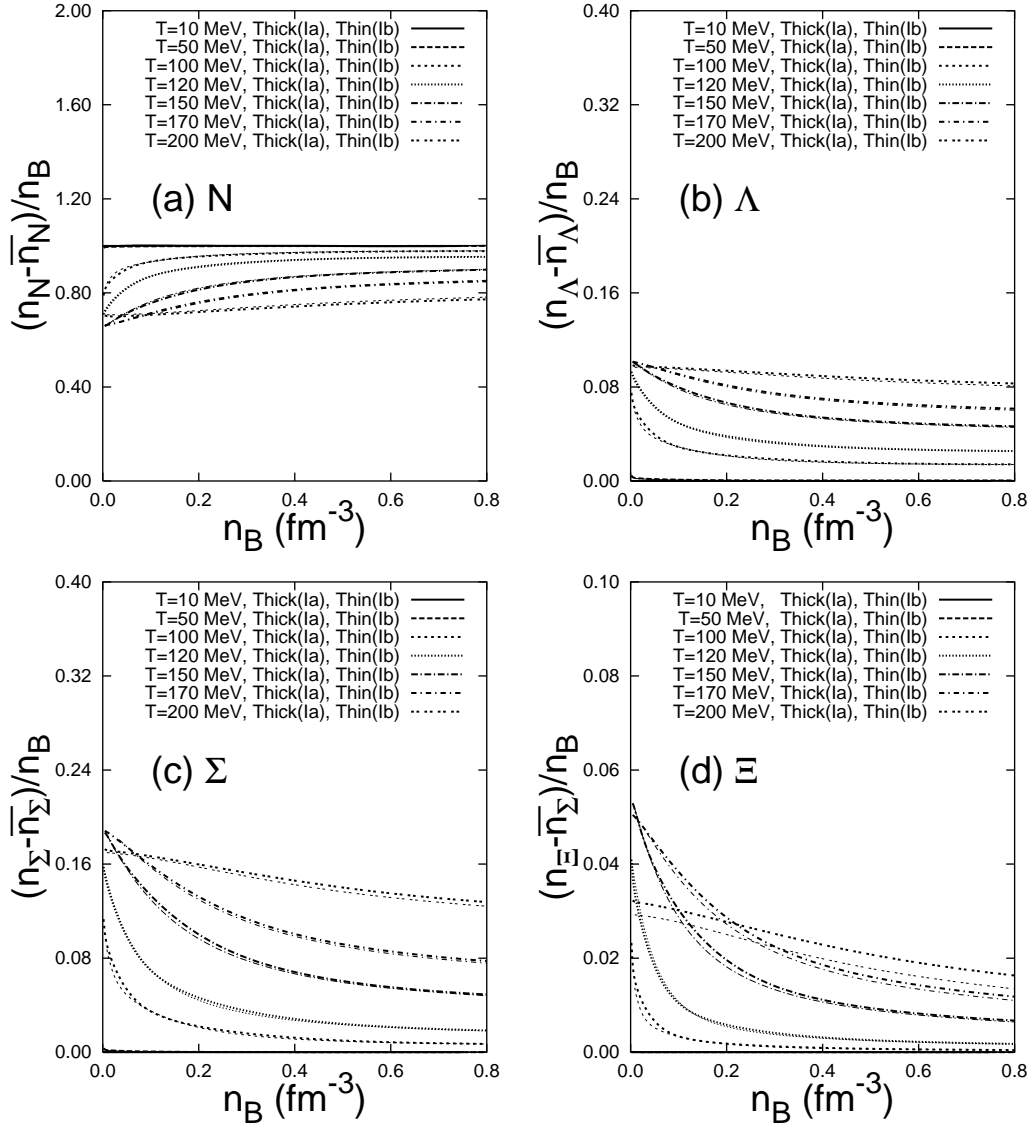


FIG. 7: The density fraction for baryon and anti-baryon species n_i/n_B vs baryon density n_B with several temperatures using the fitting set Fits (Ia) and (Ib). a) $x_N = (n_N - \bar{n}_N)/n_B$, b) $x_\Lambda = (n_\Lambda - \bar{n}_\Lambda)/n_B$, c) $x_\Sigma = (n_\Sigma - \bar{n}_\Sigma)/n_B$, d) $x_\Xi = (n_\Xi - \bar{n}_\Xi)/n_B$.

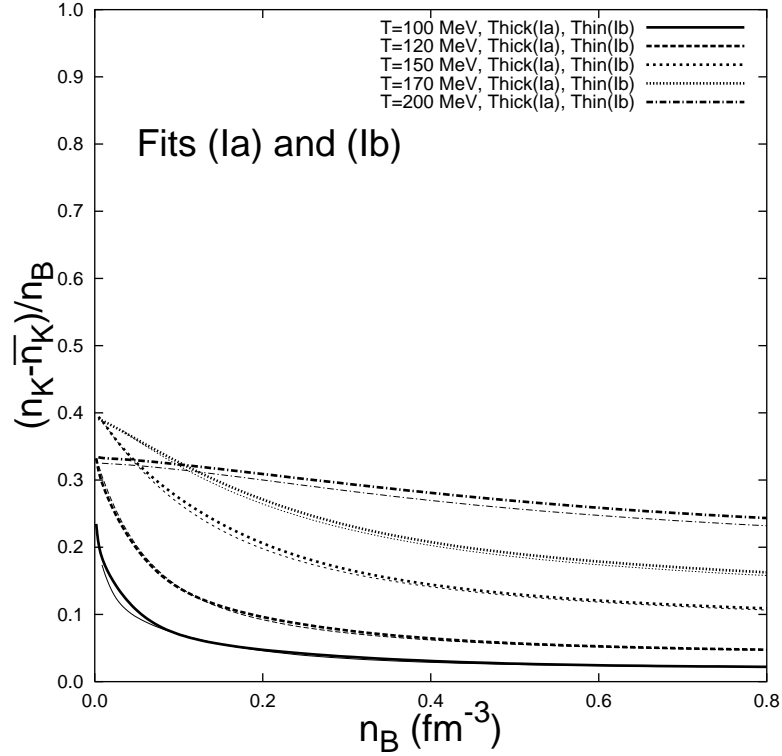


FIG. 8: Same as Fig.(3) but using the fitting sets (Ia) and (Ib).

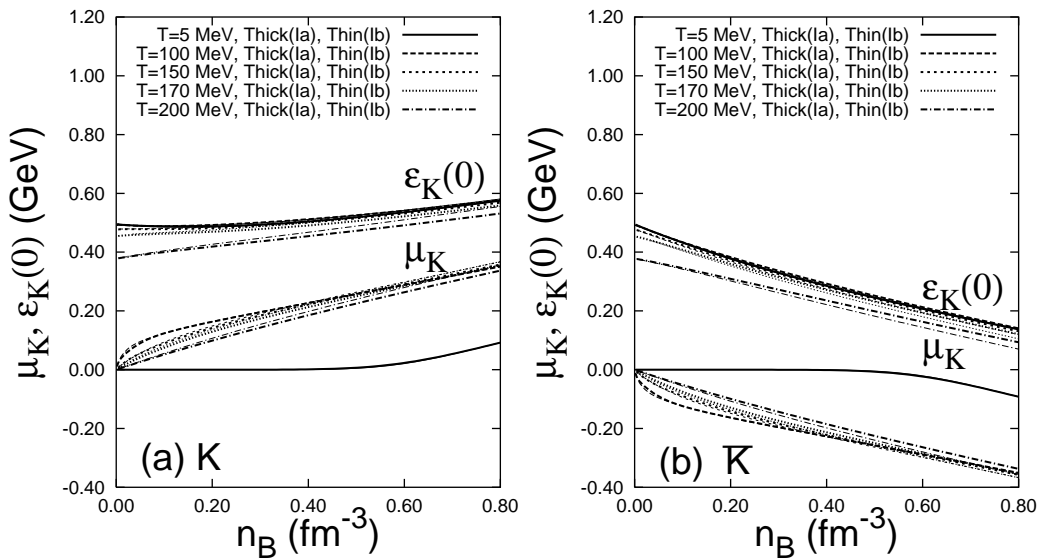


FIG. 9: Same as Fig.(4) but using the fitting sets (Ia) and (Ib).

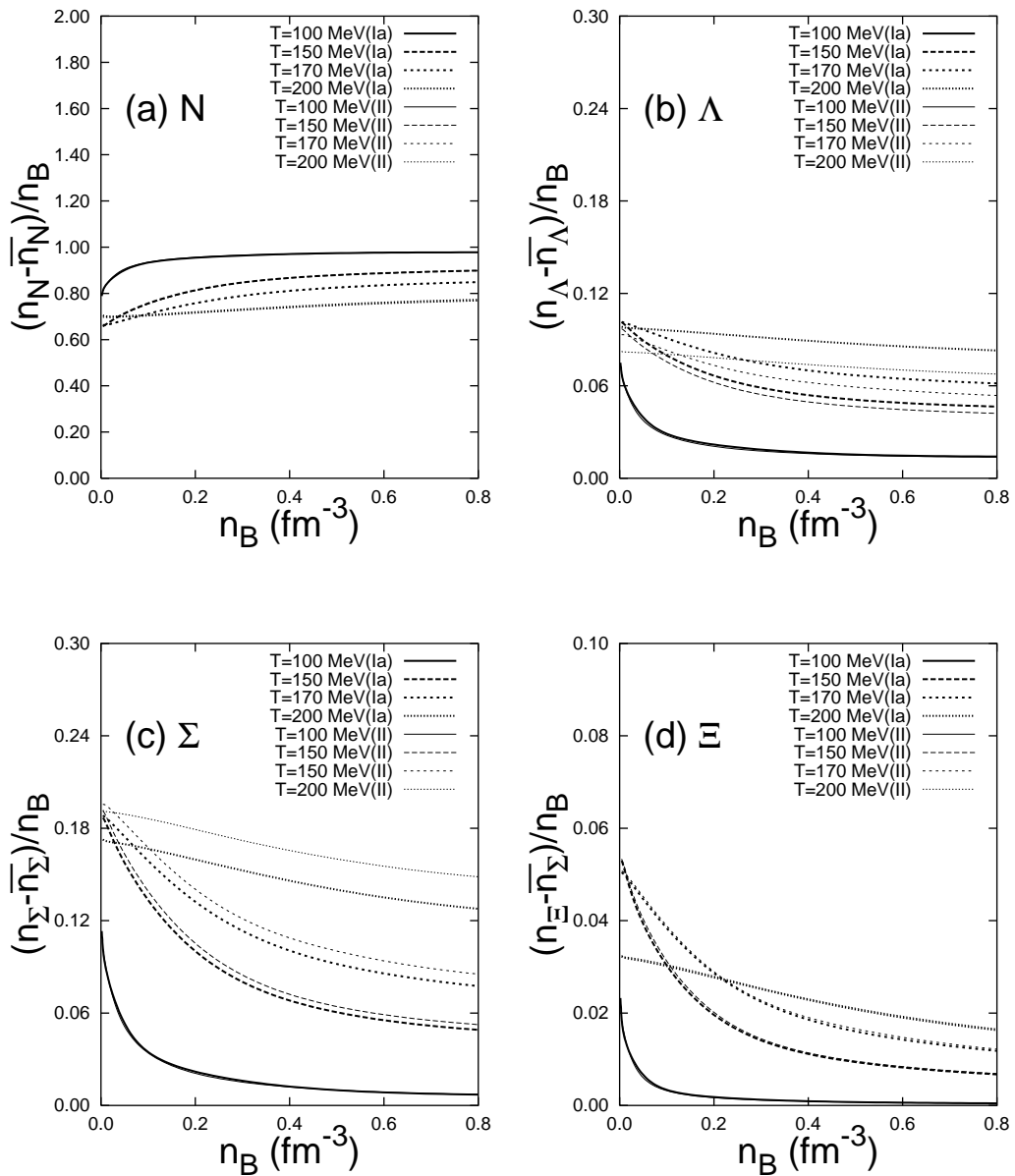


FIG. 10: Same as Fig.(2) but using fitting sets (Ia) and (II).

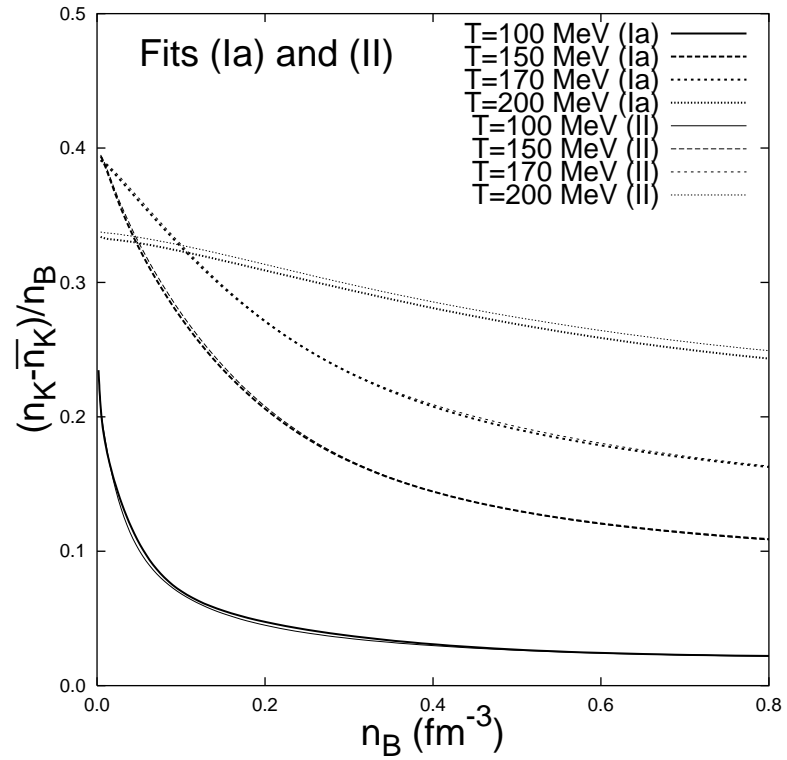


FIG. 11: Same as Fig.(2) but using the fitting sets (Ia) and (II).

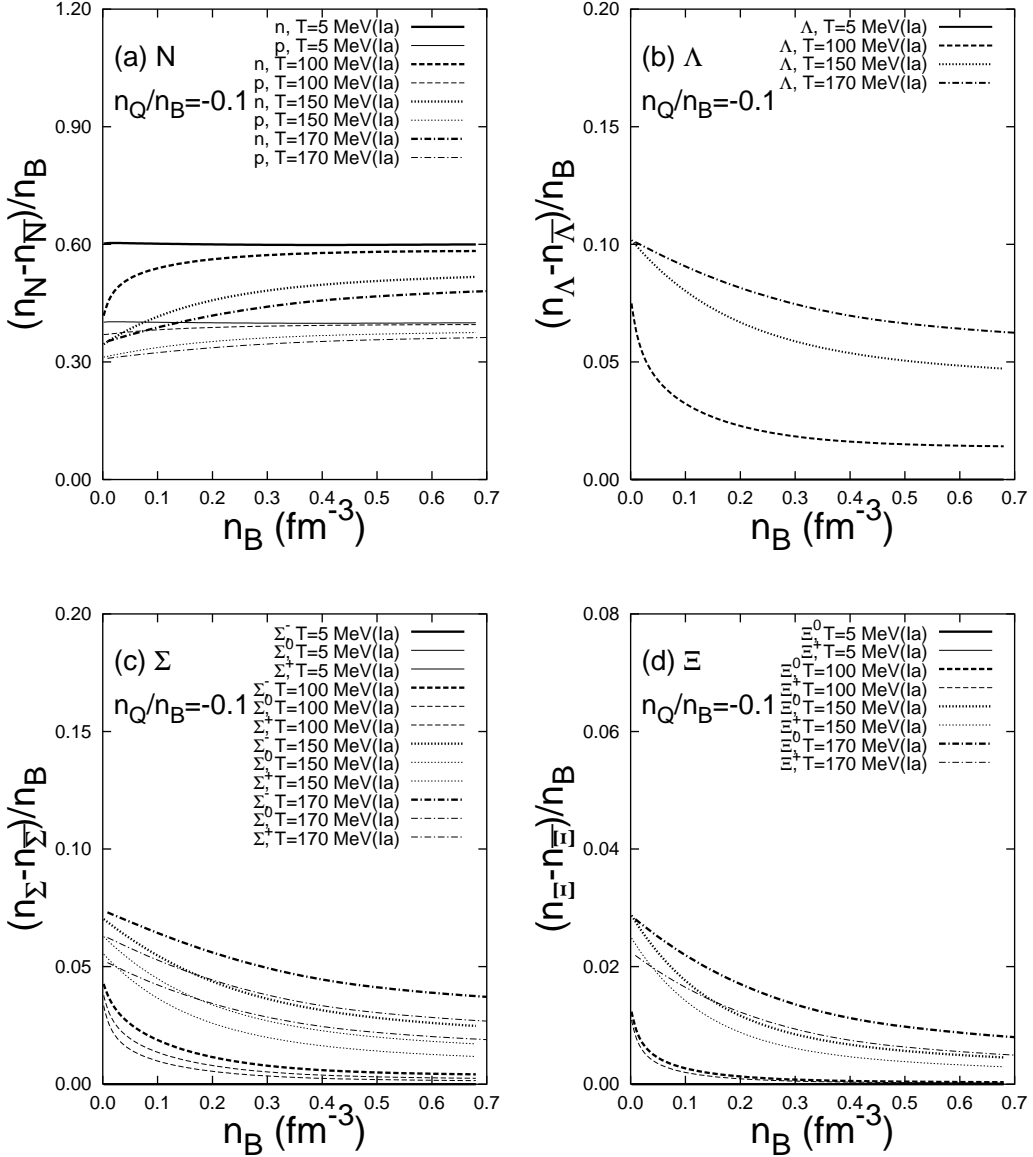


FIG. 12: The density fraction $x_i = (n_i - \bar{n}_i)/n_B$ for baryon species i versus baryon density n_B for $n_Q/n_B = -0.1$ for several temperatures using the fitting set (Ia). a) N , b) Λ , c) Σ , d) Ξ .

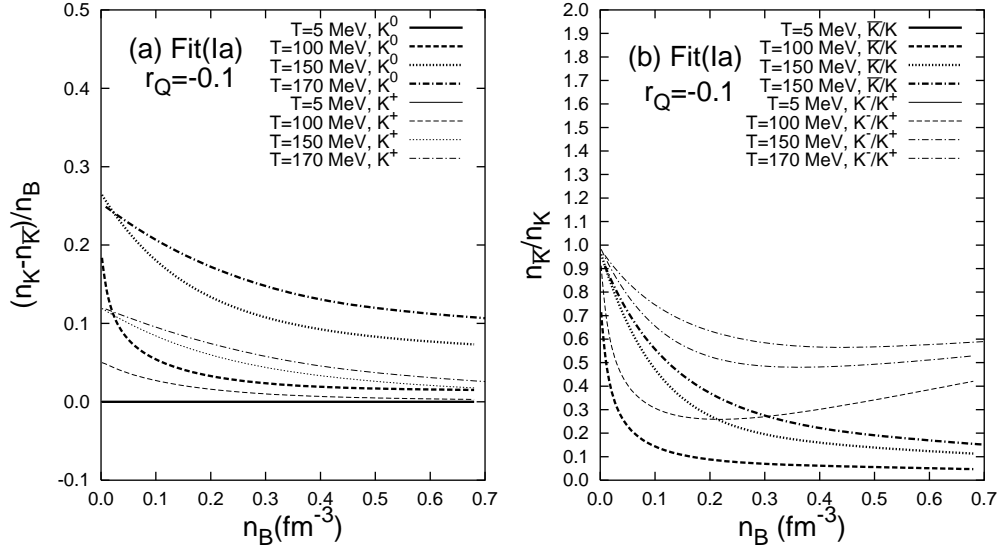


FIG. 13: Kaon abundance vs baryon density n_B for various temperatures for $n_Q/n_B = -0.1$ using the fitting set (Ia). a) The ratio of anti-kaon abundance over kaon abundance $n_{\bar{K}}/n_K$, b) The kaon density fraction $x_k = (n_K - n_{\bar{K}})/n_B$.

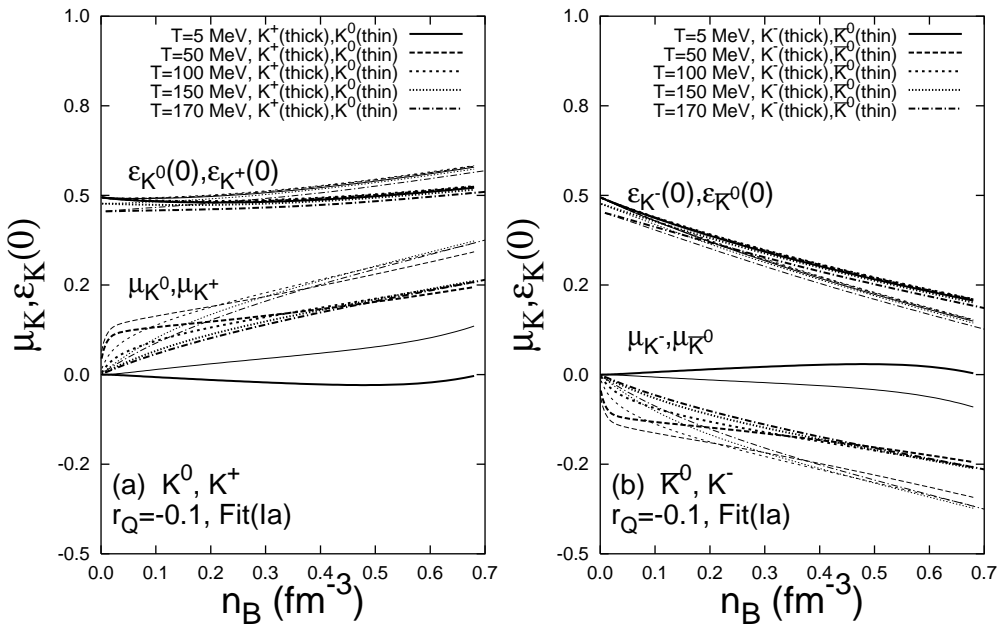


FIG. 14: The strange chemical potential μ_S and the kaon threshold effective energy $\epsilon_k^*(0)$ versus baryon density n_B at various temperatures for $n_Q/n_B = -0.1$ using the fitting set (Ia). a) Kaons, b) Anti-kaons.

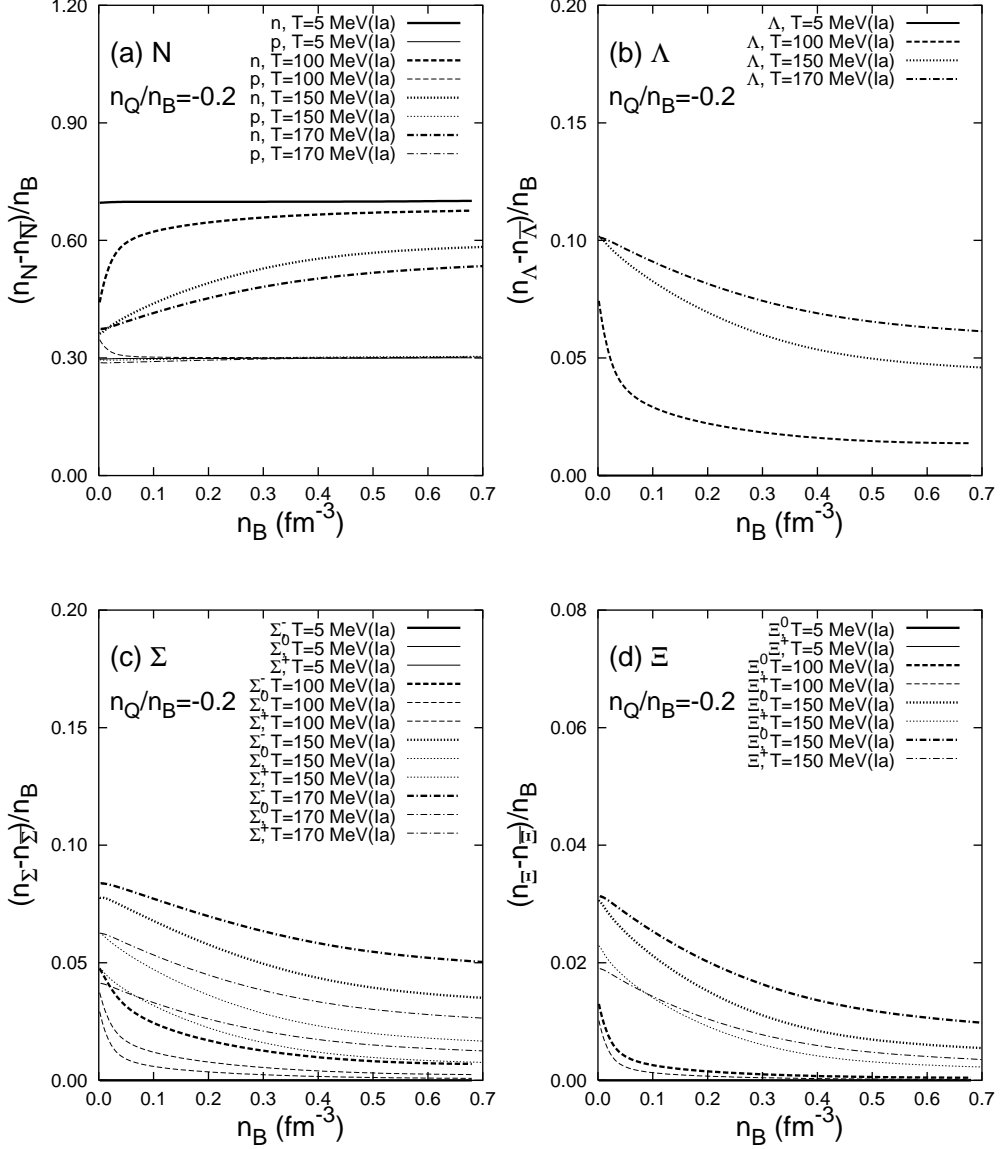


FIG. 15: The density fraction $x_i = (n_i - \bar{n}_i)/n_B$ for baryon species i versus baryon density n_B for $n_Q/n_B = -0.2$ at several temperatures using the fitting set (Ia). a) N , b) Λ , c) Σ , d) Ξ .

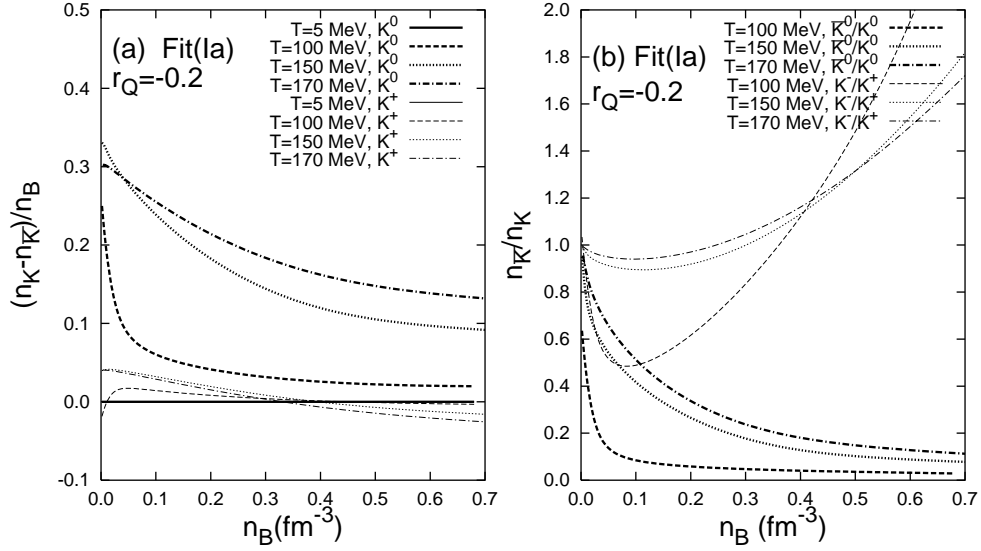


FIG. 16: The kaon abundance vs baryon density n_B at various temperatures for $n_Q/n_B = -0.2$ using the fitting set (Ia). a) The ratio of anti-kaon abundance over kaon abundance $n_{\bar{K}}/n_K$, b) The kaon density fraction $x_k = (n_K - n_{\bar{K}})/n_B$.

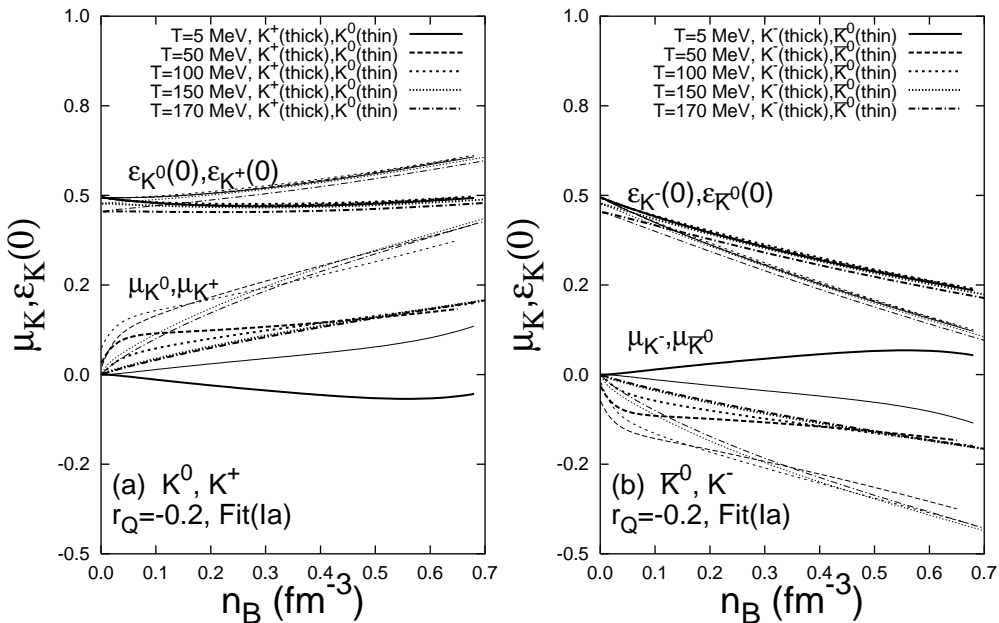


FIG. 17: The strange chemical potential μ_S and the kaon threshold effective energy $\epsilon_k^*(0)$ versus baryon density n_B with various temperatures for $n_Q/n_B = -0.2$ using the fitting set Fit(Ia). a) Kaons, b) Anti-kaons.

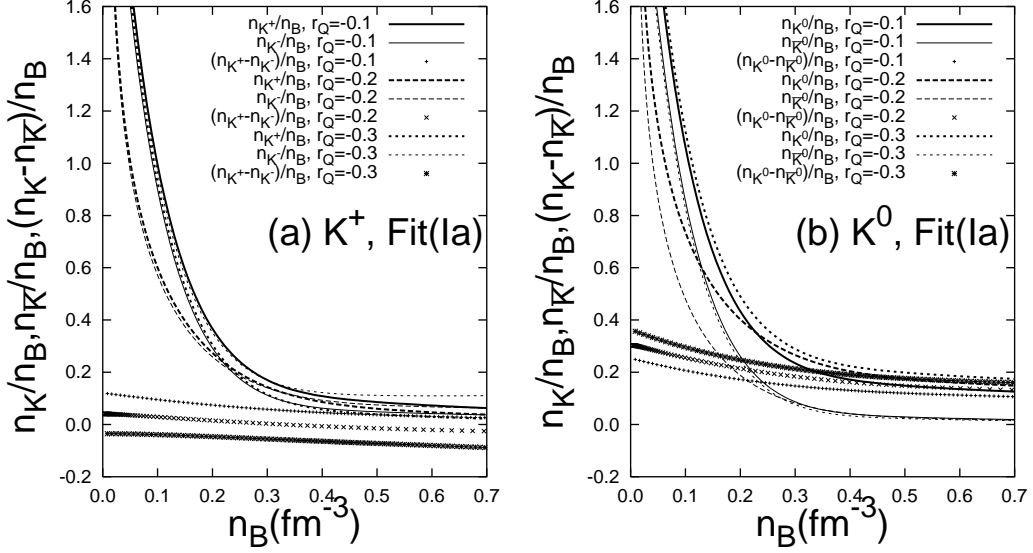


FIG. 18: The kaon and anti-kaon abundances vs baryon density n_B at temperature $T = 170$ MeV and for various charge ratios n_Q/n_B using the fitting set (Ia). a) for the charged kaons, b) for the neutral kaons. In each figure, the upper curves give the abundances n_K/n_B and $n_{\bar{K}}/n_B$ for kaon and anti-kaon, respectively, while the lower curves give the kaon density fraction $x_k = (n_K - n_{\bar{K}})/n_B$.

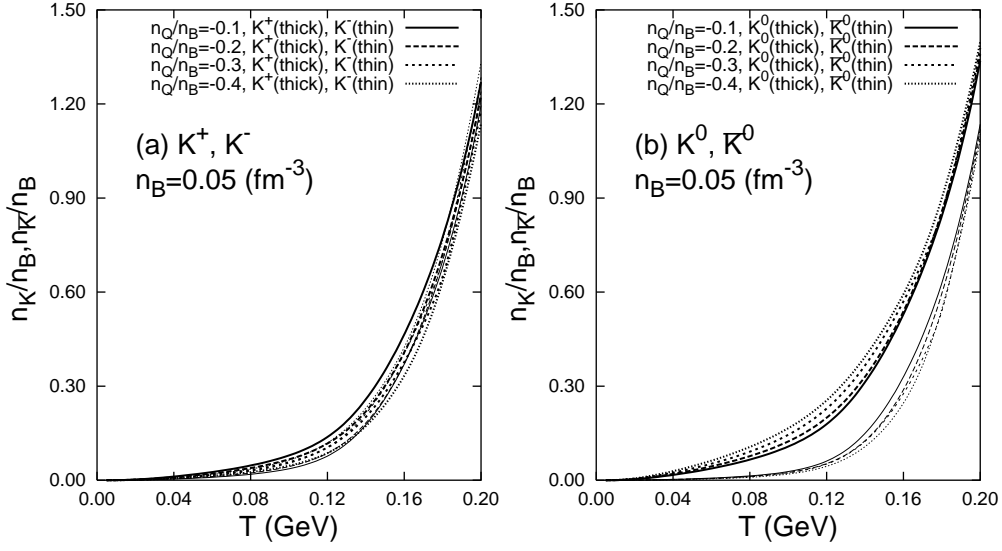


FIG. 19: The density fraction for kaon and anti-kaon versus temperature at baryon density $n_B = 0.05(\text{fm}^{-3})$ and various isospin charge ratio n_Q/n_B using the fitting set (Ia). a) K^+, K^- , b) K^0, \bar{K}^0 .

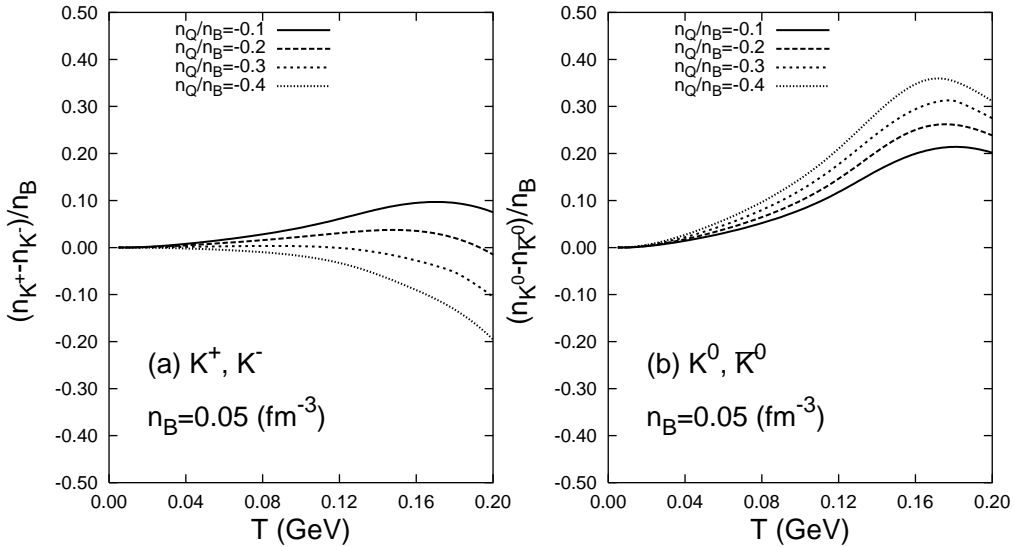


FIG. 20: The net density fraction for kaon versus temperature at baryon density $n_B = 0.05(\text{fm}^{-3})$ and various isospin charge ratio n_Q/n_B using the fitting set (Ia). a) K^+, K^- , b) K^0, \bar{K}^0 .

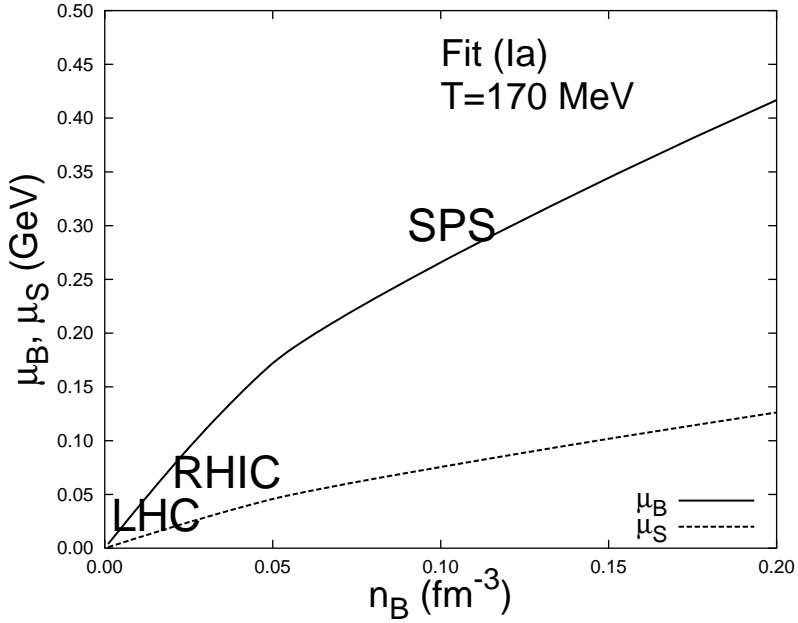


FIG. 21: The baryon and strange chemical potentials μ_B and μ_S , respectively, versus baryonic density n_B at temperature $T = 170\text{MeV}$ and low densities.

Tables

TABLE I: Fitting parameters

Fit set	$g_{q\sigma}$	$g_{q\omega}$	$g_{q\rho}$	$g_{N\sigma}^{\text{bag}}$	$g_{\Lambda\sigma}^{\text{bag}}$	$g_{\Lambda\sigma^*}^{\text{bag}}$	$g_{\Sigma\sigma}^{\text{bag}}$	$g_{\Sigma\sigma^*}^{\text{bag}}$	$g_{\Xi\sigma}^{\text{bag}}$	$g_{\Xi\sigma^*}^{\text{bag}}$	$g_{K\sigma}^{\text{bag}}$	$g_{K\sigma^*}^{\text{bag}}$
Model I	1.0	2.705	8.086	6.81	4.22	5.45	1.63	7.26	2.27	9.12	2.27	$\sqrt{2} \times 2.27$
Model II	1.0	2.705	8.086	6.81	4.22	0.0	1.63	10.28	2.27	10.17	2.27	$\sqrt{2} \times 2.27$